

Mixed-mode oscillations in a three time-scale model for the dopaminergic neuron

Martin Krupa^{a)}

Department of Mathematical Sciences, New Mexico State University, P.O. Box 30001, Department 3MB, Las Cruces, New Mexico 88003, USA

Nikola Popović^{b)} and Nancy Kopell^{c)}

Center for BioDynamics and Department of Mathematics and Statistics, Boston University, 111 Cummington Street, Boston, Massachusetts 02215, USA

Horacio G. Rotstein^{d)}

Department of Mathematical Sciences, New Jersey Institute of Technology, University Heights, Newark, New Jersey 07102, USA

(Received 7 March 2007; accepted 31 July 2007; published online 27 March 2008)

Mixed-mode dynamics is a complex type of dynamical behavior that has been observed both numerically and experimentally in numerous prototypical systems in the natural sciences. The compartmental Wilson-Callaway model for the dopaminergic neuron is an example of a system that exhibits a wide variety of mixed-mode patterns upon variation of a control parameter. One characteristic feature of this system is the presence of multiple time scales. In this article, we study the Wilson-Callaway model from a geometric point of view. We show that the observed mixed-mode dynamics is caused by a slowly varying canard structure. By appropriately transforming the model equations, we reduce them to an underlying three-dimensional canonical form that can be analyzed via a slight adaptation of the approach developed by M. Krupa, N. Popović, and N. Kopell (unpublished). © 2008 American Institute of Physics. [DOI: 10.1063/1.2779859]

Dopamine is a neurotransmitter that is synthesized by so-called dopaminergic neurons in the brain. The dopaminergic neurons of the mammalian brain stem are believed to play a role in movement, cognition, motivation, and reward. Traditional models for this type of neuron¹ have assumed the presence of different ionic mechanisms in the soma and the dendrites. Wilson and Callaway² have proposed a coupled oscillator model where these ionic mechanisms are the same throughout the neuron, but where the natural frequency of oscillation varies: The individual oscillators correspond to neuronal compartments, with the compartments representing the soma and proximal dendrites of the neuron having much lower natural frequencies than those representing the more distal regions. More recently, Medvedev and Cisternas,³ as well as Medvedev *et al.*,⁴ have studied a simplified version of this Wilson-Callaway model. They observed the so-called mixed-mode oscillatory behavior, a complex type of dynamics that is characterized by a mixture of small-amplitude oscillations and large-amplitude (relaxation) excursions. Moreover, Medvedev and Cisternas³ gave an explanation for this dynamics based on the so-called canard mechanism.^{5,6} In the present article, we extend the analysis of Ref. 3 in the sense that we prove how the version of the Wilson-Callaway model analyzed in Ref. 3 can be reduced rigorously to a canonical, three-

dimensional, three time-scale system formulated in Ref. 7. This reduction is based on geometric singular perturbation theory and geometric desingularization, and allows us to make precise predictions on the mixed-mode dynamics of the original model.

I. INTRODUCTION

Wilson and Callaway² studied N -chains of strongly electrically coupled relaxation oscillators to describe the dynamics of membrane potential and calcium concentration in dopaminergic neurons in the mammalian brain stem. The compartmental model analyzed by Medvedev and Cisternas³ is slightly simpler, and is given by the following $2N$ -dimensional system of equations:

$$\varepsilon \frac{dv_i}{dt} = g_1(v_i)(E_1 - v_i) + g_2(u_i)(E_2 - v_i) + \bar{g}_3(E_3 - v_i) + d(v_{i+1} - 2v_i + v_{i-1}), \quad (1a)$$

$$\frac{du_i}{dt} = \omega_i \left(g_1(v_i)(E_1 - v_i) - \frac{u_i}{\tau} \right), \quad (1b)$$

with $i=1, \dots, N$, $v_0 \equiv v_1$, and $v_{N+1} \equiv v_N$. [Note that, in contrast to the original Wilson-Callaway equations, Eqs. (1a) and (1b) are nondimensionalized, and that the coupling is assumed to be symmetric rather than anisotropic.] The variables v_i and u_i in Eqs. (1a) and (1b) stand for the voltage and calcium concentration in the i th compartment, respectively. The first three terms in Eq. (1a) represent intrinsic currents: A voltage-gated calcium current, a calcium-gated potassium

^{a)}Electronic mail: mkrupa@nmsu.edu.

^{b)}Electronic mail: popovic@math.bu.edu.

^{c)}Electronic mail: nk@math.bu.edu.

^{d)}Electronic mail: rotstein@oak.njit.edu.

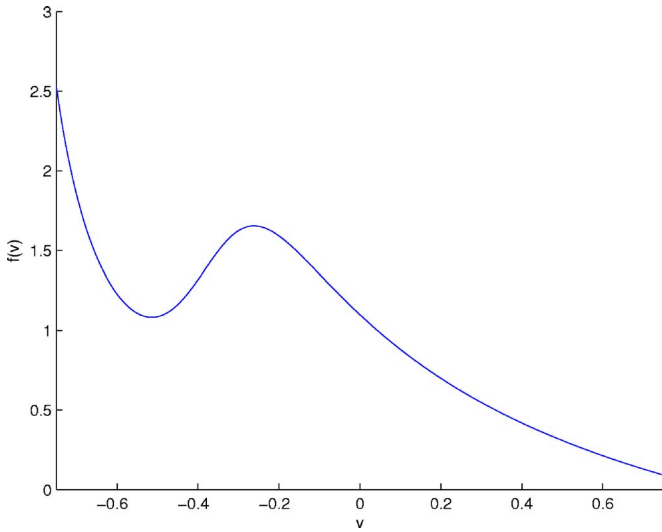


FIG. 1. (Color online) The function f in Eqs. (3a)–(3d).

current, and a leak current. The corresponding conductances are given by $g_1(v_i)$, $g_2(u_i)$, and \bar{g}_3 , respectively, with

$$g_1(v_i) = \frac{\bar{g}_1}{1 + e^{-(v_i - c_1)/c_2}} \quad \text{and} \quad g_2(u_i) = \frac{\bar{g}_2 u_i^4}{u_i^4 + c_3^4}. \quad (2)$$

Here, E_j , \bar{g}_j , and c_j ($j=1, \dots, 3$) are real constants, cf. Ref. 3 and the Appendix. The last term in Eq. (1a) models the electrical coupling between adjacent compartments, where the coupling strength d is assumed to be large ($d \gg 1$). Finally, ε is a small parameter ($0 < \varepsilon \ll 1$).

For the sake of simplicity, we restrict ourselves to the two-compartment case here, i.e., we only consider Eqs. (1a) and (1b) with $N=2$. Also, following Ref. 3, we approximate $g_2(u_i)$ by its linearization about $u_i=2$ in Eqs. (1a) and (1b): $g_2(u_i) \approx -au_i + b$. Hence, in sum, we will be concerned with the following system of equations:

$$\varepsilon \dot{v}_1 = a(E_2 - v_1)[f(v_1) - u_1] + d(v_2 - v_1), \quad (3a)$$

$$\varepsilon \dot{v}_2 = a(E_2 - v_2)[f(v_2) - u_2] + d(v_1 - v_2), \quad (3b)$$

$$\dot{u}_1 = \omega_1 \left(g_1(v_1)(E_1 - v_1) - \frac{u_1}{\tau} \right), \quad (3c)$$

$$\dot{u}_2 = \omega_2 \left(g_1(v_2)(E_1 - v_2) - \frac{u_2}{\tau} \right), \quad (3d)$$

where the function $f(v_i)$ is defined as

$$f(v_i) = \frac{g_1(v_i)(E_1 - v_i) + \bar{g}_3(E_3 - v_i)}{a(E_2 - v_i)} + \frac{b}{a},$$

cf. Ref. 4, p. 339, and the overdot denotes differentiation with respect to t . Note that in the parameter range of interest to us, the graph of f has a qualitatively cubic form, see Fig. 1. In particular, we assume that E_j , \bar{g}_j , and c_j are chosen such that f is non-negative in the physiologically relevant regime. The values of the parameters in Eqs. (3a)–(3d) are specified in detail in the Appendix, see also Ref. 3.

Clearly, under the above assumptions, Eqs. (3a)–(3d) are a four-dimensional fast-slow system in standard form, with two fast variables (v_1 and v_2) and two slow variables (u_1 and u_2). One principal finding in Ref. 3 is the occurrence of *mixed-mode oscillations* (MMOs) in Eqs. (3a)–(3d) upon variation of the control parameter τ , which physiologically corresponds to the rate of calcium efflux. In the resulting time series of v_i , small-amplitude oscillations typically alternate with large-amplitude excursions (“spikes”). MMOs are frequently observed in multiple-scale systems of differential equations, such as Eqs. (1a) and (1b). Consequently, the amplitudes of the mixed-mode patterns found in such systems often vary over several orders of magnitude; see Figs. 2–4 for an illustration.

Various mechanisms have been brought forward to explain the emergence of MMOs in fast-slow systems; see, e.g., Ref. 7 for a detailed discussion. Recently, a potentially more unified approach has emerged, namely the so-called “(generalized) canard mechanism.” This idea, which was formulated by Milik and Szmolyan in the context of the autocatalator,^{5,8} has subsequently been extended by a number of authors.^{6,9–11} In fact, it was shown in Ref. 3 that the mixed-mode behavior observed in Eqs. (3a)–(3d) indeed arises via the canard mechanism.

To date, canard-induced MMOs have been studied predominantly in three-dimensional systems with one fast and two slow variables, or in systems that can at least be reduced to this setting; cf. Refs. 6–9 and 12. A prototypical system of this type is given as follows:

$$v' = -z + f(v), \quad (4a)$$

$$z' = \varepsilon(v - w), \quad (4b)$$

$$w' = \varepsilon[\mu + \phi(v, z, w)]. \quad (4c)$$

Here, $f(v) = f_2 v^2 + f_3 v^3 + \mathcal{O}(v^4)$ with f_2 and f_3 real and constant, $\mu > 0$ is a real parameter, and $\phi(v, z, w) = \mathcal{O}(v, z, w)$ is some smooth function.

It is very natural to attempt a reduction of Eqs. (3a)–(3d) to a system of the form of Eqs. (4a)–(4c), since the strong diffusive coupling makes v_1 and v_2 essentially indistinguishable. Medvedev and Cisternas³ perform such a reduction and obtain a hybrid system with two continuous variables, corresponding to v and z in Eqs. (4a)–(4c), and one discrete variable, which they call the “update constant” K . This reduction is rigorously justified by the results of Medvedev and Kopell,¹³ who prove the existence of a global strongly attracting three-dimensional invariant manifold \mathcal{M} for Eqs. (3a)–(3d). In this article, we show that, in suitable coordinates, \mathcal{M} can be interpreted as a globally attracting *slow manifold* of a fast-slow system with singular parameter $\delta = d^{-1}$; consequently, its existence can be deduced from Fenichel theory.¹⁴ Moreover, we introduce a continuous variable w in the process, which is a slowly varying analog of the constant K defined in Ref. 3. An additional coordinate transformation, after restriction of Eqs. (3a)–(3d) to \mathcal{M} , then leads us to a system that is of a form very similar to Eqs. (4a)–(4c). One major difference between this system and Eqs. (4a)–(4c) lies in the fact that the variable w is signifi-

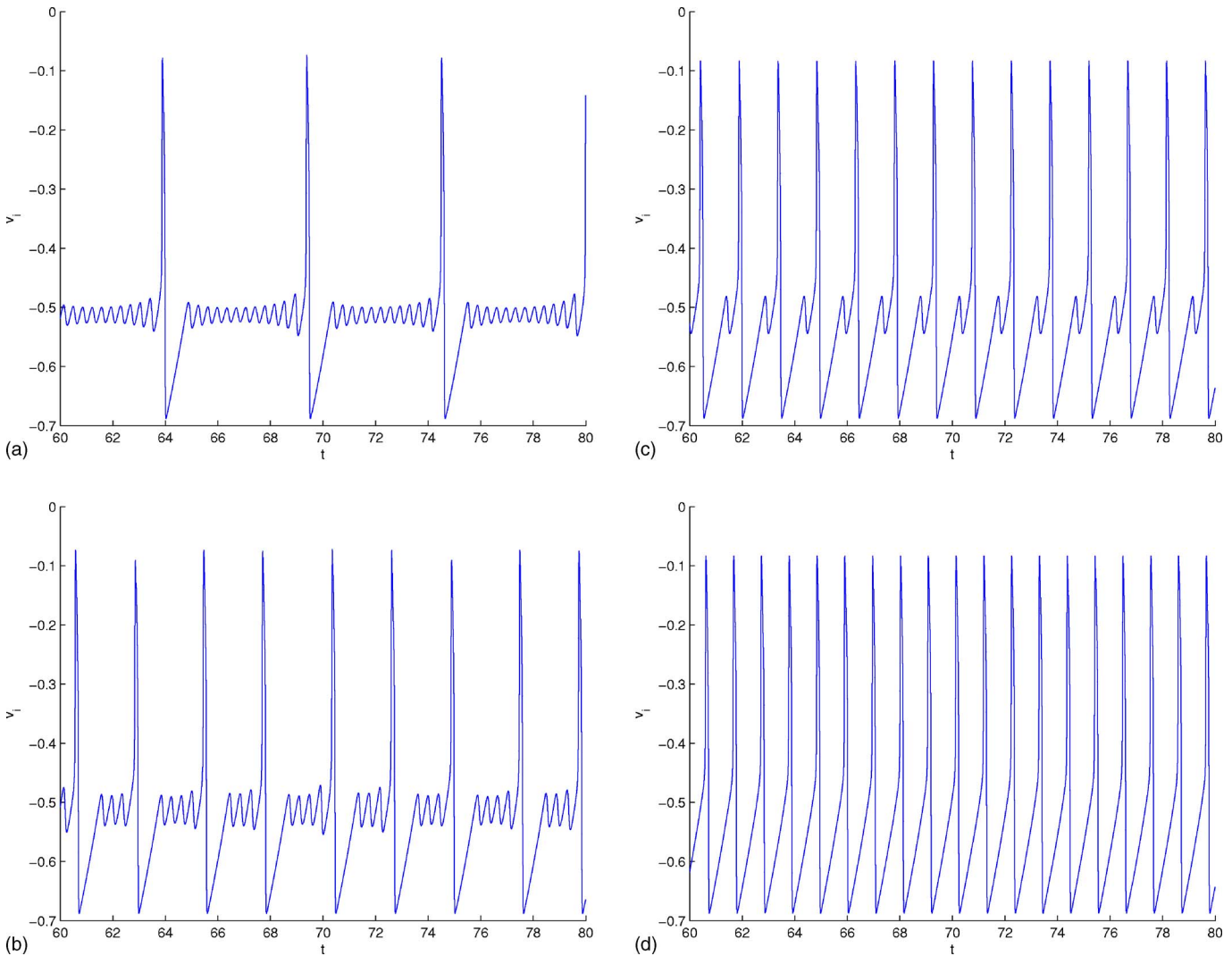


FIG. 2. (Color online) Mixed-mode dynamics for $\omega_2=16$ in Eqs. (3a)–(3d): (a) $\tau=9.7$; (b) $\tau=9.3$; (c) $\tau=8.9$; (d) $\tau=8.5$.

cantly slower than z and, hence, that there are three time scales present in the former. In Ref. 7, we have studied canard-induced MMOs in the family of three-dimensional three time-scale systems given by

$$v' = -z + f_2 v^2 + f_3 v^3, \tag{5a}$$

$$z' = \varepsilon(v - w), \tag{5b}$$

$$w' = \varepsilon^2(\mu - g_1 z). \tag{5c}$$

[Note that v , z , and w are fast, slow, and “superslow,” by Eqs. (5a)–(5c), respectively.] We have shown that, due to its three time-scale structure, Eqs. (5a)–(5c) can be interpreted as a near-integrable system, in the sense that it is a small perturbation of the two-dimensional (v, z) subsystem in Eqs. (5a)–(5c). This subsystem, in turn, is a prototypical example of a system that undergoes a so-called canard explosion upon variation of w . Using this observation, we have been able to explain the mixed-mode dynamics of Eqs. (5a)–(5c) as arising via “slow passage through a canard explosion.” Details on the classical canard phenomenon in the context of two-dimensional fast-slow systems can be found in Refs. 15–18.

In the remainder of this article, we show how the three-dimensional, reduced system obtained from Eqs. (3a)–(3d) after restriction to \mathcal{M} can be fitted into the framework of Eqs. (5a)–(5c), and how the results obtained in Ref. 7 can be adapted to investigate its dynamics. Due to the different powers of ε that will arise in our scaling of Eqs. (3a)–(3d), the resulting system will differ somewhat from Eqs. (5a)–(5c). However, we will prove that the same analysis can still be applied. Consequently, our conclusions on the mixed-mode patterns observed in Eqs. (3a)–(3d) will be in close analogy to those presented in Ref. 7 in the context of Eqs. (5a)–(5c).

To that end, we note that MMO periodic orbits can be characterized by their so-called *Farey sequence* $L_0^{k_0} L_1^{k_1} \dots L_j^{k_j}$, which encodes the number of large-amplitude excursions L_j and the number of small-amplitude oscillations k_j , respectively, associated with the given orbit. We will show that for ε sufficiently small, the stable dynamics of Eqs. (3a)–(3d) is dominated by sequences that are composed of segments of the form 1^k , 1^{k-1} , and 1^{k-2} . Moreover, we will obtain an analytic estimate of the width of the relevant parameter (μ) interval on which MMOs occur, see Eq. (40)

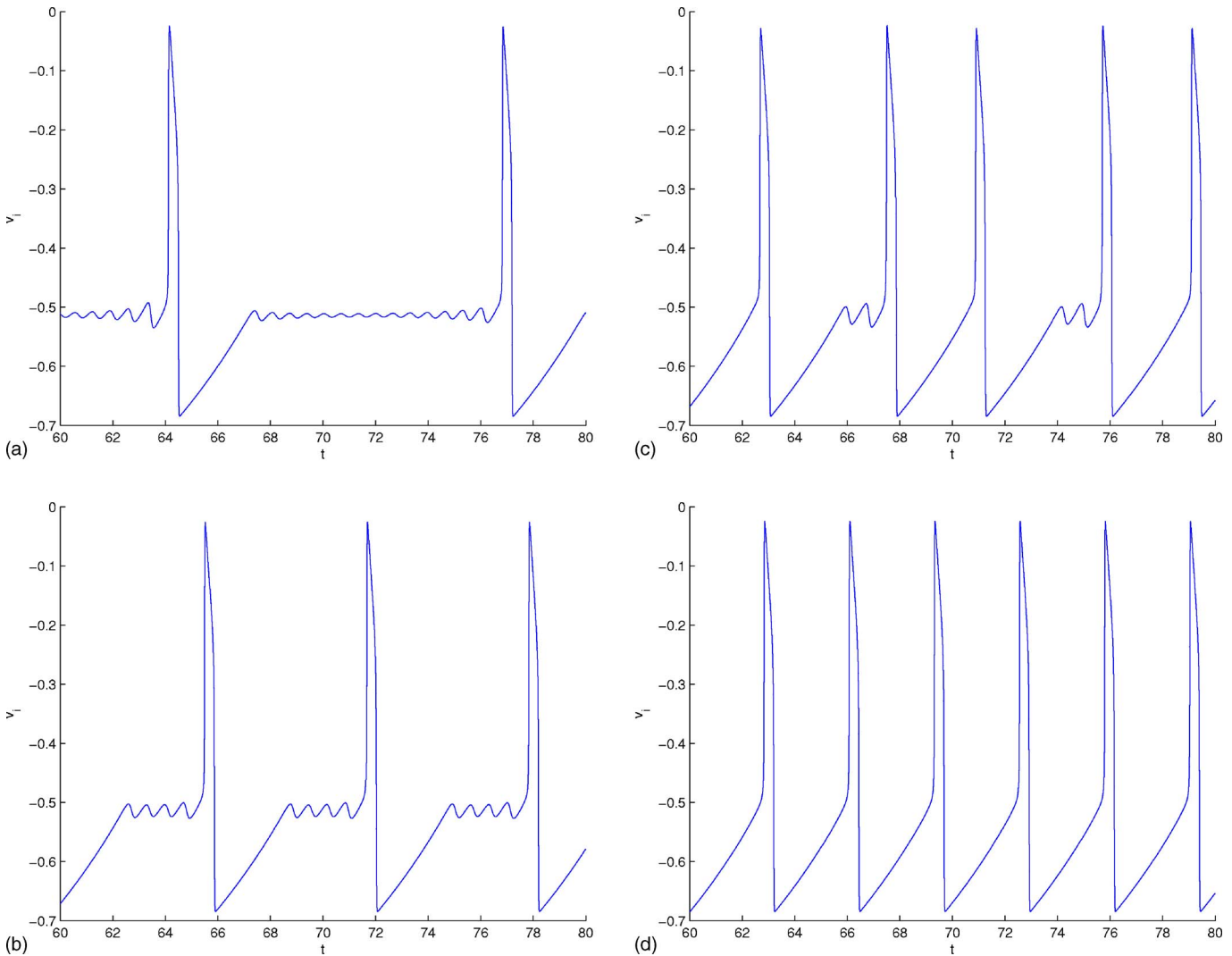


FIG. 3. (Color online) Mixed-mode dynamics for $\omega_2=4$ in Eqs. (3a)–(3d): (a) $\tau=10.0$; (b) $\tau=9.8$; (c) $\tau=9.6$; (d) $\tau=9.4$.

below; here, $\mu=\tau^{-1}$. Similarly, the stability interval of 1^k -type orbits will turn out to be $\mathcal{O}[\varepsilon^{3/4}(-\ln \varepsilon)^{-(1/2)}]$ wide. Hence, our analysis is an extension of the results of Ref. 3: There, careful numerics was used to show that Eqs. (3a)–(3d) display a variety of MMOs with varying τ . However, the analysis in Ref. 3 does not provide any explicit results on what Farey sequences can be expected to occur, on what their ordering will be, or on what the size of the corresponding parameter intervals is.

Given that our predictions are based on the leading-order asymptotics of Eqs. (3a)–(3d), they agree quite well with the numerics, especially in the case considered in Ref. 3, where $\omega_1=1$ and $\omega_2=16$. We discuss the bifurcation structure of Eqs. (3a)–(3d) in detail only in that case here; however, we will indicate how our results could be extended to the more general case in which ω_1 and ω_2 do not necessarily differ by an order of magnitude. Figures 2–4 show a sample of the mixed-mode patterns that occur in Eqs. (3a)–(3d) for different values of ω_2 (16, 4, and 1.5), with $\omega_1=1$ fixed.

This article is organized as follows: In Sec. II, we reduce the four-dimensional system in Eqs. (3a)–(3d) to a three-dimensional one, via a global reduction to a center manifold

\mathcal{M} that can be interpreted as a strongly attracting slow manifold. The resulting system is of the type of Eqs. (4a)–(4c); such systems are frequently analyzed by reducing their dynamics to the *critical manifold* defined by $z=f(v)$ in Eqs. (4a)–(4c), and by characterizing the equilibria of the resulting, planar equations.¹⁹ At the end of Sec. II, we briefly outline this approach in the present context. Then, in Sec. III, we reformulate the reduced, three-dimensional system on \mathcal{M} to identify its three time-scale structure, and to fit it into the framework of Eqs. (5a)–(5c). In particular, we indicate how geometric singular perturbation theory can be combined with geometric desingularization to derive asymptotic formulas for the return map induced by the flow of Eqs. (5a)–(5c). These formulas, in turn, allow us to characterize the mixed-mode dynamics of the original, full system in Eqs. (3a)–(3d). Notably, the structure of the bifurcation (Farey) sequences observed in Eqs. (3a)–(3d) is determined by the presence of so-called *secondary canards*; an in-depth discussion of these notions can be found in Ref. 7. Finally, in Sec. IV, we summarize and discuss our results, and we illustrate them numerically.

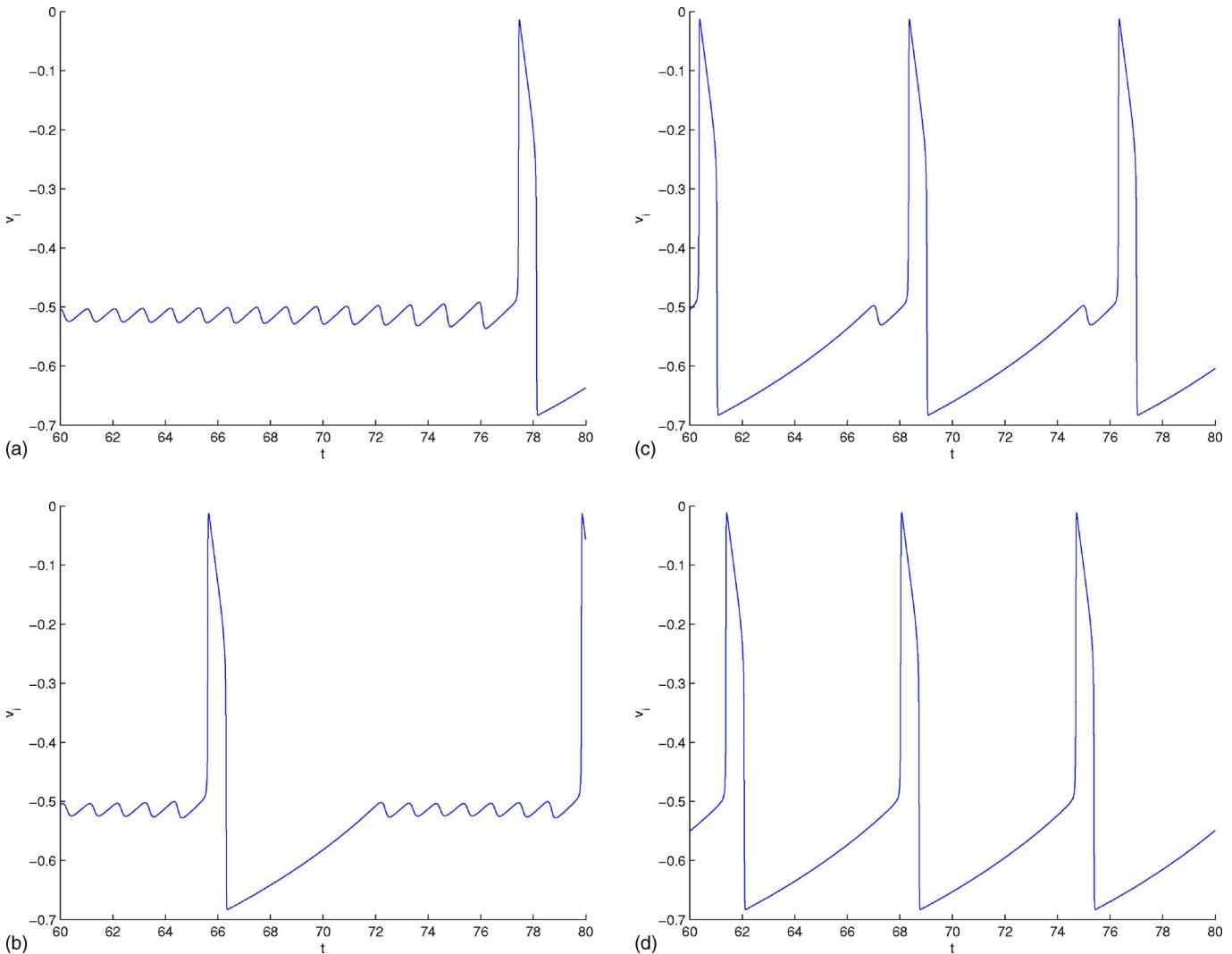


FIG. 4. (Color online) Mixed-mode dynamics for $\omega_2=1.5$ in Eqs. (3a)–(3d): (a) $\tau=10.19$; (b) $\tau=10.16$; (c) $\tau=10.13$; (d) $\tau=10.1$.

II. GLOBAL CENTER MANIFOLD REDUCTION

The results of Ref. 3 strongly indicate the existence of a global invariant (center) manifold \mathcal{M} for Eqs. (3a)–(3d) in the limit of strong coupling. This conclusion is based on the following property of Eqs. (3a)–(3d): For $d > 0$ sufficiently large, i.e., for $\delta := d^{-1} \ll 1$, there exists some $t_0 > 0$ such that

$$v_2(t) - v_1(t) = \mathcal{O}(\delta) \quad \text{for all } t \geq t_0 \tag{6}$$

as long as the corresponding trajectories remain uniformly bounded. A proof of Eq. (6) is given in Ref. 13, Theorem 7.1, in the simplified setting of chains of coupled FitzHugh-Nagumo oscillators.

The idea that a global center manifold reduction for Eqs. (3a)–(3d) is possible will allow us to eliminate one of the fast (v_i) variables from the problem. More specifically, we postulate that \mathcal{M} is defined by the condition

$$v_2 = v_1 + \delta \tilde{\vartheta}(v_1, u_1, u_2, \varepsilon, \delta), \tag{7}$$

where $\tilde{\vartheta}$ is a smooth function, possibly depending on ε and δ , but bounded as $\varepsilon, \delta \rightarrow 0$; see Ref. 4, Eq. (3.9). We will prove that this postulate follows by standard Fenichel

theory¹⁴ once suitable coordinates have been introduced in Eqs. (3a)–(3d). The manifold \mathcal{M} will contain the relevant dynamics of Eqs. (3a)–(3d), in the sense that it will be a global attractor for the corresponding flow.

A. Center manifold as a slow manifold

We first show that there is an additional (superfast) time scale in Eqs. (3a)–(3d) that is associated with the relaxation of the system to its global, three-dimensional center manifold \mathcal{M} .²⁰ The resulting fast-slow structure, which has to be superimposed on the scale decomposition induced by the small parameter ε , will allow us to describe \mathcal{M} as a slow manifold after appropriately reformulating Eqs. (3a)–(3d). [This contrasts with the approach in Refs. 3 and 13, where Eq. (6) was established via a hierarchy of detailed asymptotic estimates.]

We begin by rewriting Eqs. (3a)–(3d) in terms of the fast time $\tilde{t} = t/\varepsilon$,

$$v_1' = a(E_2 - v_1)[f(v_1) - u_1] + d(v_2 - v_1), \tag{8a}$$

$$v_2' = a(E_2 - v_2)[f(v_2) - u_2] + d(v_1 - v_2), \tag{8b}$$

$$u'_1 = \varepsilon \omega_1 \left(g_1(v_1)(E_1 - v_1) - \frac{u_1}{\tau} \right), \tag{8c}$$

$$u'_2 = \varepsilon \omega_2 \left(g_1(v_2)(E_1 - v_2) - \frac{u_2}{\tau} \right). \tag{8d}$$

Given that \mathcal{M} must, to leading order, be given by $v_2 = v_1$, we introduce the sum and difference variables

$$x = \frac{v_1 - v_2}{2} \quad \text{and} \quad y = \frac{v_1 + v_2}{2} \tag{9}$$

in Eqs. (8a)–(8d).

Now, let

$$h_1(x, y, u_1, u_2) = \frac{1}{2} \{ a[E_2 - (x + y)][f(x + y) - u_1] - a[E_2 - (-x + y)][f(-x + y) - u_2] \},$$

$$h_2(x, y, u_1, u_2) = \frac{1}{2} \{ a[E_2 - (x + y)][f(x + y) - u_1] + a[E_2 - (-x + y)][f(-x + y) - u_2] \};$$

then, Eqs. (8a) and (8b) become

$$x' = -2dx + h_1(x, y, u_1, u_2),$$

$$y' = h_2(x, y, u_1, u_2).$$

Dividing the first equation by d , we obtain

$$\delta x' = -2x + \delta h_1(x, y, u_1, u_2), \tag{10}$$

$$y' = h_2(x, y, u_1, u_2),$$

which is a singularly perturbed system in its slow formulation, with singular parameter δ . The corresponding critical manifold \mathcal{M}_0 obtained for $\delta=0$ is given by $\{x=0\}$. Note that \mathcal{M}_0 is clearly normally hyperbolic; hence, standard geometric singular perturbation (Fenichel) theory is applicable.¹⁴

Taking into account Eqs. (8c) and (8d), the fast system corresponding to Eqs. (10) is given by

$$\begin{aligned} \dot{x} &= -2x + \delta h_1(x, y, u_1, u_2), \\ \dot{y} &= \delta h_2(x, y, u_1, u_2), \end{aligned} \tag{11}$$

$$\dot{u}_1 = \varepsilon \delta \omega_1 \left(g_1(v_1)(E_1 - v_1) - \frac{u_1}{\tau} \right),$$

$$\dot{u}_2 = \varepsilon \delta \omega_2 \left(g_1(v_2)(E_1 - v_2) - \frac{u_2}{\tau} \right),$$

where the overdot now denotes differentiation with respect to the new fast time. With x defined as in Eq. (9), an approximation for $\tilde{\vartheta}$ can be obtained by writing the slow manifold for Eqs. (11) in the form

$$x = \delta \hat{\vartheta}(y, u_1, u_2, \varepsilon, \delta) \tag{12}$$

and by computing the asymptotic expansion of $\hat{\vartheta}$ in powers of δ ,

$$\hat{\vartheta}(y, u_1, u_2, \varepsilon, \delta) = \sum_{j=0}^{\infty} \delta^j \hat{\vartheta}_j(y, u_1, u_2, \varepsilon). \tag{13}$$

To that end, we first differentiate Eq. (12) with respect to time and then make use of Eqs. (8a)–(8d) and (11) to derive the invariance condition

$$\begin{aligned} & -2\delta \hat{\vartheta} + h_1(\delta \hat{\vartheta}, y, u_1, u_2) \\ &= \delta \left[\frac{\partial \hat{\vartheta}}{\partial y} h_2(\delta \hat{\vartheta}, y, u_1, u_2) \right. \\ & \quad + \frac{\partial \hat{\vartheta}}{\partial u_1} \varepsilon \omega_1 \left(g_1(\delta \hat{\vartheta} + y)[E_1 - (\delta \hat{\vartheta} + y)] - \frac{u_1}{\tau} \right) \\ & \quad \left. + \frac{\partial \hat{\vartheta}}{\partial u_2} \varepsilon \omega_2 \left(g_1(-\delta \hat{\vartheta} + y)[E_1 - (-\delta \hat{\vartheta} + y)] - \frac{u_2}{\tau} \right) \right]. \end{aligned} \tag{14}$$

We now substitute Eq. (13) in Eq. (14), equate like powers of δ , and solve the resulting equations inductively. To leading order, we find

$$\hat{\vartheta}_0 = \frac{1}{2} [h_1(0, y, u_1, u_2)]_0,$$

where $[h_j]_k$ denotes the terms of order k in the Taylor expansion of h_j in δ around $x=0$. It now follows from

$$f(\pm \delta \hat{\vartheta} + y) = f(y) \pm \delta \hat{\vartheta} f'(y) + \mathcal{O}(\delta^2)$$

that $[h_1]_0 = \frac{1}{2} a(E_2 - y)[f(y) - u_1 - f(y) + u_2]$, and, hence, that

$$\hat{\vartheta}_0(y, u_1, u_2, \varepsilon) = -\frac{a}{4} (E_2 - y)(u_1 - u_2). \tag{15}$$

Note that to lowest order, there is no ε dependence in $\hat{\vartheta}$.

Remark 1. One can proceed in a similar manner to determine the first-order correction $\hat{\vartheta}_1$ in Eq. (13). As it turns out, $\hat{\vartheta}_1$ does depend on ε , in contrast to $\hat{\vartheta}_0$. In fact, we expect that all subsequent terms in Eq. (13) will also be ε dependent.

In terms of the original variables v_1 and v_2 , we find

$$\begin{aligned} v_2 &= v_1 + \delta \frac{a}{2} (E_2 - v_1)(u_1 - u_2) + \mathcal{O}(\delta^2) \\ &= v_1 + \delta \tilde{\vartheta}_0(v_1, u_1, u_2, \varepsilon) + \mathcal{O}(\delta^2) \end{aligned} \tag{16}$$

from Eq. (15), with $\tilde{\vartheta}_0(v_1, u_1, u_2, \varepsilon) = \tilde{\vartheta}(v_1, u_1, u_2, \varepsilon, 0)$. As we will show, it suffices to consider this lowest-order approximation for $\tilde{\vartheta}$ in order to reproduce qualitatively the results of Ref. 3.

B. Preliminary transformation of Eqs. (3a)–(3d)

We now modify Eqs. (3a)–(3d) as follows: First, we define the new variable

$$w = \frac{\omega_2 u_1 - \omega_1 u_2}{\omega_1 + \omega_2};$$

then, we use the ansatz in Eq. (7); finally, we note that, given Eq. (7) and

$$g_1(v_1 + \delta\tilde{\vartheta}(v_1, u_1, u_2, \varepsilon, \delta)) = g_1(v_1) + \delta\tilde{\vartheta}(v_1, u_1, u_2, \varepsilon, 0) \times g_1'(v_1) + \mathcal{O}(\delta^2),$$

we obtain

$$g_1(v_1)(E_1 - v_1) - g_1(v_2)(E_1 - v_2) = \delta\tilde{\vartheta}(v_1, u_1, u_2, \varepsilon, 0)[g_1(v_1) - g_1'(v_1) \times (E_1 - v_1)] + \mathcal{O}(\delta^2).$$

With these definitions, Eqs. (3a)–(3d) become

$$\varepsilon\dot{v}_1 = a(E_2 - v_1)[f(v_1) - u_1] + \vartheta(v_1, u_1, w, \varepsilon, \delta),$$

$$\dot{u}_1 = \omega_1 \left(g_1(v_1)(E_1 - v_1) - \frac{u_1}{\tau} \right), \tag{17}$$

$$\dot{w} = \frac{\omega_1\omega_2}{\omega_1 + \omega_2} \delta \{ \vartheta(v_1, u_1, w, \varepsilon, 0) \times [g_1(v_1) - g_1'(v_1)(E_1 - v_1)] + \mathcal{O}(\delta) \} - \frac{\omega_2}{(\omega_1 + \omega_2)\tau} [(\omega_1 - \omega_2)u_1 + (\omega_1 + \omega_2)w],$$

where $\vartheta(v_1, u_1, w, \varepsilon, \delta) = \tilde{\vartheta}(v_1, u_1, u_2, \varepsilon, \delta)$ now. In particular, by making use of the definition of w to eliminate u_2 from Eq. (16), we find

$$\vartheta(v_1, u_1, w, \varepsilon, 0) = \frac{a}{2\omega_1} (E_2 - v_1) [(\omega_1 - \omega_2)u_1 + (\omega_1 + \omega_2)w] \tag{18}$$

for the leading-order asymptotics of ϑ .

Remark 2. The introduction of w is motivated by the definition of the constant K in Ref. 3. In fact, our analysis shows that w is a continuous analog of K . Moreover, it is obvious that ϑ has to depend on w , see Eq. (18), whereas Ref. 4, Eq. (3.9), suggests no such dependence on K .

Substituting Eq. (18) in Eqs. (17), we find that for $\delta=0$,

$$\varepsilon\dot{v}_1 = a(E_2 - v_1) \left(f(v_1) + \frac{\omega_1 + \omega_2}{2\omega_1} (-u_1 + w) \right), \tag{19a}$$

$$\dot{u}_1 = \omega_1 \left(g_1(v_1)(E_1 - v_1) - \frac{u_1}{\tau} \right), \tag{19b}$$

$$\dot{w} = - \frac{\omega_2}{(\omega_1 + \omega_2)\tau} [(\omega_1 - \omega_2)u_1 + (\omega_1 + \omega_2)w]. \tag{19c}$$

Equations (19a)–(19c) are of the type considered in Ref. 19 with one fast variable v_1 and two slow variables u_1 and w . Now, we note that the prefactor $a(E_2 - v_1)$ in Eq. (19a) is always nonzero on physiological grounds. [More precisely, $a(E_2 - v_1) > 0$, since we are only interested in $E_2 - v_1 < 0$ and since $a < 0$ by assumption, cf. the Appendix.] Hence, it follows that the corresponding critical manifold for Eqs. (19a)–(19c), obtained in the singular limit of $\varepsilon=0$, is defined by

$$\left(f(v_1) + \frac{\omega_1 + \omega_2}{2\omega_1} (-u_1 + w) \right) = 0.$$

Alternatively, this manifold, which we denote by \mathcal{S}_0 , can be represented as

$$u_1 = \phi(v_1, w) := \frac{\omega_1}{\bar{\omega}} f(v_1) + w, \tag{20}$$

where $\bar{\omega} = (\omega_1 + \omega_2)/2$ is the arithmetic mean of ω_1 and ω_2 . Note that Eq. (20) is identical to the expression obtained in Ref. 4, Eq. (3.13), with K there replaced by the new variable w here. Hence, w can be considered a continuous analog of K that varies on the slow time scales defined by δ and τ^{-1} .

Finally, in analogy to Ref. 4, Eq. (3.7), we can define the so-called ‘‘coupling current’’ between the two compartments in Eqs. (17) by

$$\tilde{c}(v_1, u_1, u_2, \varepsilon, \delta) = - \frac{\tilde{\vartheta}(v_1, u_1, u_2, \varepsilon, \delta)}{a(E_2 - v_1)}.$$

Here, we have used $d(v_2 - v_1) = \tilde{\vartheta}$, cf. Eq. (7). In particular, for $\delta \rightarrow 0$, it follows from Eq. (20) after some calculation that

$$c(v_1, u_1, w, \varepsilon, 0) := \tilde{c}(v_1, u_1, u_2, \varepsilon, 0) = \frac{\omega_1 - \omega_2}{\omega_1 + \omega_2} f(v_1) + w$$

to leading order, in analogy to Ref. 4, Eq. (3.12).

To simplify the subsequent analysis, we introduce a new variable z in Eqs. (19a)–(19c), with

$$z = \frac{\bar{\omega}}{\omega_1} (u - w).$$

[Here and in the following, we omit the subscripts 1 in (v_1, u_1) for the sake of readability.] In terms of (v, z, w) , Eqs. (19a)–(19c) are transformed to

$$\varepsilon\dot{v} = a(E_2 - v)[f(v) - z], \tag{21a}$$

$$\dot{z} = \bar{\omega}g_1(v)(E_1 - v) - \frac{\omega_1^2 + \omega_2^2}{\tau(\omega_1 + \omega_2)}z - \frac{\omega_1 - \omega_2}{2\tau}w, \tag{21b}$$

$$\dot{w} = - \frac{\omega_1\omega_2}{\tau\bar{\omega}} \left(\frac{\omega_1 - \omega_2}{\omega_1 + \omega_2}z + w \right). \tag{21c}$$

These are the equations that will be studied now. In particular, in the context of Eqs. (21a)–(21c), the critical manifold \mathcal{S}_0 is defined by the constraint $f(v) - z = 0$.

C. Reduced equations for Eqs. (21a)–(21c)

In this subsection, we briefly outline how the so-called *reduced equations*^{10,19} for Eqs. (21a)–(21c) can be derived. These equations are obtained in the singular limit of $\varepsilon=0$ in Eqs. (21a)–(21c) and can be interpreted as a planar system of differential equations with phase space given by the critical manifold \mathcal{S}_0 ,

$$0 = f(v) - z, \tag{22a}$$

$$\dot{z} = \bar{\omega}g_1(v)(E_1 - v) - \frac{\omega_1^2 + \omega_2^2}{\tau(\omega_1 + \omega_2)}z - \frac{\omega_1 - \omega_2}{2\tau}w, \tag{22b}$$

$$\dot{w} = -\frac{\omega_1\omega_2}{\tau\bar{\omega}}\left(\frac{\omega_1 - \omega_2}{\omega_1 + \omega_2}z + w\right). \tag{22c}$$

[Here, we recall that $a(E_2 - v) > 0$ in Eqs. (21a)–(21c) and, hence, that this prefactor can be canceled for $\varepsilon = 0$.] The motivation for studying the reduced system (22a)–(22c) is to locate so-called *folded equilibria*, which are essential for classifying the canard dynamics of Eqs. (21a)–(21c).

Now, recall that the function f in Eq. (22a) has a qualitatively cubic form, cf. again Fig. 1. Consequently, $f'(v) = 0$ vanishes for exactly two values of v , which we denote by v^+ and v^- ; numerically, one finds $v^+ \approx -0.2618$ and $v^- \approx -0.5141$ for the parameter values specified in the Appendix. We will denote the two *fold lines* where $v = v^\pm$ is constant by ℓ^\pm , respectively, and we observe that ℓ^\pm are lines of equilibria for Eqs. (22a)–(22c).

Next, we note that $f'(v) < 0$ for $v < v^-$ and $v > v^+$, as well as that $f'(v) > 0$ for $v^- < v < v^+$. Hence, for (v, z, w) in some closed and bounded subset of \mathbb{R}^3 , the critical manifold \mathcal{S}_0 will consist of two attracting sheets, $\mathcal{S}_0^{\pm} : \{v < v^\pm\}$ and $\mathcal{S}_0^{\pm} : \{v > v^\pm\}$, and a repelling one, $\mathcal{S}_0^{\pm} : \{v^- < v < v^+\}$, with the respective boundaries given by ℓ^\pm . By standard singular perturbation (Fenichel) theory,¹⁴ these sheets will perturb, smoothly in ε for $\varepsilon > 0$ sufficiently small, to sheets $\mathcal{S}_\varepsilon^{\pm}$, $\mathcal{S}_\varepsilon^{\pm}$, and $\mathcal{S}_\varepsilon^{\pm}$ of the slow manifold \mathcal{S}_ε that are unique up to exponentially small terms in ε . [In other words, away from ℓ^\pm , the reduced dynamics of Eqs. (22a)–(22c) is a good approximation for the full dynamics of Eqs. (21a)–(21c).]

Finally, we discuss the dynamics of Eqs. (22a)–(22c) near the fold lines ℓ^\pm . A typical point on the fold is characterized by the property that solutions reaching it in forward or backward time cannot be continued as solutions of Eqs. (22a)–(22c). For the dynamics of Eqs. (21a)–(21c), this implies that solutions passing near such points have to leave the slow-evolution regime close to \mathcal{S}_0 and undergo relaxation; in other words, they leave the vicinity of the fold under the fast flow of Eqs. (21a)–(21c). So-called folded equilibria, on the other hand, are special, in that an entire family of solutions of Eqs. (22a)–(22c) can in fact pass through the fold at these points; see, e.g., Ref. 19. In the following subsection, we will briefly discuss folded equilibria in the context of Eqs. (21a)–(21c). A more detailed discussion can be found in the article by Jalics *et al.*,²¹ which will also be included in the present issue.

D. Folded equilibria for Eqs. (21a)–(21c)

To find folded equilibria for Eqs. (21a)–(21c), we follow the procedure outlined in Ref. 10. Since we are projecting Eqs. (22a)–(22c) onto \mathcal{S}_0 , or, equivalently, onto the (v, w) plane, we begin by eliminating any z dependence from the equations. Making use of the constraint in Eq. (22a), we substitute $z = f(v)$ and $\dot{z} = f'(v)\dot{v}$ in Eqs. (22a)–(22c) to obtain

$$f'(v)\dot{v} = \bar{\omega}g_1(v)(E_1 - v) - \frac{1}{4\tau\bar{\omega}}[2(\omega_1^2 + \omega_2^2)f(v) + (\omega_1^2 - \omega_2^2)w], \tag{23a}$$

$$\dot{w} = -\frac{\omega_1\omega_2}{\tau\bar{\omega}}\left(\frac{\omega_1 - \omega_2}{\omega_1 + \omega_2}f(v) + w\right). \tag{23b}$$

Next, we perform a trajectory-dependent time rescaling which introduces the factor $-f'(v)$ in the right-hand sides of Eqs. (23a) and (23b). Canceling this factor in Eq. (23a), we find

$$\dot{v} = -\bar{\omega}(E_1 - v)g_1(v) + \frac{1}{4\tau\bar{\omega}}[2(\omega_1^2 + \omega_2^2)f(v) + (\omega_1^2 - \omega_2^2)w], \tag{24a}$$

$$\dot{w} = \frac{\omega_1\omega_2}{\tau\bar{\omega}}f'(v)\left(\frac{\omega_1 - \omega_2}{\omega_1 + \omega_2}f(v) + w\right), \tag{24b}$$

where the overdot now denotes differentiation with respect to the new rescaled time. The expression in brackets in Eq. (24b) is precisely the coupling current c .³

Remark 3. Similar results can be obtained from the full (four-dimensional) fast-slow system (3a)–(3d) via the alternative approach outlined in Ref. 6.

Equilibria of Eqs. (24a) and (24b) now correspond to folded equilibria of the original Eqs. (21a)–(21c). These equilibria are classified according to their character as equilibrium points of the rescaled planar system (24a) and (24b), i.e., according to the local dynamics of the reduced flow near the fold. [Note, however, that folded equilibria are generally not equilibria for the original reduced equations in Eqs. (23a) and (23b).] Here, we are especially interested in *folded nodes* and *folded saddle nodes*; see Ref. 19 for details. Typically, this type of folded equilibria occurs in problems that exhibit mixed-mode dynamics. More precisely, the small-oscillation component of MMO time series frequently arises in a region that is limited to a folded (saddle) node.^{9,10} In fact, as we will show below, this is precisely the scenario that gives rise to the mixed-mode patterns observed in Eq. (3a)–(3d).

The equilibria of Eqs. (24a) and (24b), which we denote by (v^*, w^*) , are determined as follows: Once v^* is known, w^* is obtained by setting the right-hand side in Eq. (24a) equal to zero, which gives

$$w^* = \frac{\omega_1 + \omega_2}{\omega_1 - \omega_2}\tau(E_1 - v^*)g_1(v^*) - 2\frac{\omega_1^2 + \omega_2^2}{\omega_1^2 - \omega_2^2}f(v^*). \tag{25}$$

Note that, in contrast to v^* , the value of w^* *does* depend on τ . To characterize the corresponding equilibria, we linearize Eqs. (24a) and (24b) about (v^*, w^*) , making use of $f'(v^*) = 0$,

$$\begin{bmatrix} -\bar{\omega}[(E_1 - v^*)g_1'(v^*) - g_1(v^*)] & \frac{\omega_1^2 - \omega_2^2}{4\tau\bar{\omega}} \\ \frac{2\omega_1\omega_2}{(\omega_1 - \omega_2)\tau}f''(v^*)[\tau(E_1 - v^*)g_1(v^*) - f(v^*)] & 0 \end{bmatrix}. \tag{26}$$

Given the analysis in Ref. 3, it seems reasonable to assume that the canard phenomenon should occur near ℓ^- . In fact, as we will show below, ℓ^+ contains only jump points, i.e., points at which trajectories must leave \mathcal{S}_0 under the fast flow, at least in the parameter range relevant to us.

Hence, let P^- now denote the folded equilibrium of Eqs. (24a) and (24b) with $v^* = v^-$, where the corresponding w^* value w^- is determined from Eq. (25). Motivated by the analysis in Ref. 3, we will consider $w^- = w^-(\tau)$ for varying τ , with the values of the remaining parameters in Eq. (25) as specified in the Appendix. Note that $P^- \in \ell^-$ is a local minimum of f , see Fig. 1, which implies in particular $f''(v^-) > 0$.

Now, denote by $[\dots]_{ij}$ the (i, j) th entry in Eq. (26), and note that $[\dots]_{12} < 0$ always holds, whereas the sign of $[\dots]_{21}$ depends on the sign of $\tau(E_1 - v^*)g_1(v^*) - f(v^*)$, since the prefactor is negative for $v^* = v^-$. We are interested in the cases in which P^- is a node or a saddle node. The transition between these two occurs when $[\dots]_{21}$ changes sign, i.e., when one of the eigenvalues of Eq. (26) goes through zero and P^- undergoes a saddle-node bifurcation. From Eq. (26), one finds that the critical value τ_{sn} of τ for which $[\dots]_{21} = 0$ is given by

$$\tau_{sn} = \frac{f(v^-)}{(E_1 - v^-)g_1(v^-)}. \tag{27}$$

[A closer inspection of Eq. (26) reveals that P^- is a folded saddle node of type II,⁶ since the eigendirection corresponding to the zero eigenvalue is not tangent to ℓ^- for $\tau = \tau_{sn}$.] For the parameters as given in the Appendix, the approximate value of τ_{sn} is 10.2119, while $w^-(\tau_{sn}) \approx 0.9547$, in agreement with the findings in Ref. 3.

Finally, we need to determine whether there exist folded equilibria on the “upper” fold line ℓ^+ when Eqs. (24a) and (24b) are close to saddle-node bifurcation, i.e., for $\tau \approx \tau_{sn}$. Numerically, one finds from Eq. (25) that $w^*(\tau) \approx -0.8913\tau + 3.3346$ on ℓ^+ and, hence, that $w^*(\tau) < 0$ in the τ regime of interest to us. Since u_1 and u_2 are non-negative by assumption, it follows from the definition of w and from our choice of ω_1 and ω_2 that negative w values would correspond to unphysiological values of u_i . Hence, for our purposes, the line ℓ^+ can be regarded as consisting entirely of jump points; in other words, it plays no role in our analysis.

III. REFORMULATION OF EQS. (21a)–(21c)

In this section, we show that the mixed-mode dynamics of Eqs. (3a)–(3d) can be explained by a canard phenomenon that arises through the saddle-node bifurcation at $\tau = \tau_{sn}$ in Eqs. (21a)–(21c): For the parameter values chosen as in the Appendix, Eqs. (21a)–(21c) can be interpreted as a small perturbation of the almost integrable two-dimensional (v, z) subsystem (21a) and (21b), with w taking the role of a slowly varying parameter. The emergence of small-amplitude oscillations is then triggered by a “slow passage through a canard explosion” around $P^- \in \ell^-$. The necessary analysis is based on an adaptation of the more general results of Ref. 7 to the present context and can only be outlined here; the reader is referred to the upcoming article in Ref. 7 for details.

A. Local formulation for Eqs. (21a)–(21c)

To fit Eqs. (21a)–(21c) into a framework that is better suited for a comparison with the results of Ref. 7, we first perform a sequence of normalizing transformations about the point $P^- = (v^-, z^-, w^-)$, where v^- and w^- are defined as in Sec.

II D and $z^- = f(v^-)$. Recall that $\mu = \tau^{-1}$, and define $\gamma := g_1(v^-)(E_1 - v^-)$. Note that γ is an artificial, new parameter that will prove useful for the subsequent analysis. Next, we perform the change of variables $v \mapsto v^- + v$, $z \mapsto f(v^-) + z$, and $w \mapsto w^- + w$ to translate P^- into the origin. [As we will see, this translation is an important step in the transformation of Eqs. (21a)–(21c) into a system that is similar to the canonical form derived in Ref. 7.]

With these definitions, one obtains from Eqs. (21a)–(21c), after some elementary but lengthy algebraic manipulations, the following system of equations:

$$v' = a(E_2 - v^- - v)[-z + f_2v^2 + f_3v^3 + \mathcal{O}(v^4)], \tag{28a}$$

$$z' = \varepsilon \left(\bar{\omega}[g_{11}v + \mathcal{O}(v^2)] - \frac{\omega_1^2 + \omega_2^2}{\omega_1 + \omega_2} \mu z - \frac{\omega_1 - \omega_2}{2} \mu w \right), \tag{28b}$$

$$w' = \varepsilon \left(-2 \frac{\omega_1 \omega_2}{\omega_1 - \omega_2} \gamma + 2 \frac{\omega_1 \omega_2}{\omega_1 - \omega_2} f(v^-) \mu - 2 \frac{\omega_1 \omega_2}{\omega_1 + \omega_2} \mu w - 2 \omega_1 \omega_2 \frac{\omega_1 - \omega_2}{(\omega_1 + \omega_2)^2} \mu z \right). \tag{28c}$$

Here, f_2 and f_3 are the coefficients of the Taylor expansion of f about v^- , $g_{11} = g_1'(v^-)(E_1 - v^-) - g_1(v^-)$, and the prime again denotes differentiation with respect to the fast time \tilde{t} .

An important characteristic of the compartmental Wilson-Callaway model² is the presence of multiple time scales due to the significantly different intrinsic frequencies of adjacent neuronal compartments. Namely, it is assumed that $\omega_i \ll \omega_{i+1}$ for $i \geq 1$, cf. Sec. I. In the context of Eqs. (28a)–(28c), this assumption simplifies to $\omega_1 \ll \omega_2$; in particular, Medvedev and Cisternas³ take $\omega_1 = 1$ and $\omega_2 = 16$; see also the Appendix. An additional scale in Eqs. (28a)–(28c) is determined by the fact that μ and γ are $\mathcal{O}(\sqrt{\varepsilon})$ in the regime of interest to us: Note that $\varepsilon = 0.013$, again by the Appendix, and recall that $\mu \approx \tau_{sn}^{-1} \approx 0.1$; similarly, one can show numerically that $\gamma \approx 0.1$. To reflect these observations, we introduce the following rescaling in Eqs. (28a)–(28c):

$$\omega_2 = \frac{\tilde{\omega}_2}{\sqrt{\varepsilon}}, \quad \gamma = \sqrt{\varepsilon} \tilde{\gamma}, \quad \mu = \sqrt{\varepsilon} \tilde{\mu}. \tag{29}$$

Finally, to reduce Eqs. (28a)–(28c) as closely as possible to the canonical system (5a)–(5c) formulated in Ref. 7, we rescale w via

$$w = \frac{2}{\tilde{\omega}_2 \tilde{\mu}} \frac{\tilde{w}}{\sqrt{\varepsilon}}.$$

As a result, Eqs. (28a)–(28c) are transformed as follows:

$$v' = a(E_2 - v^- - v)[-z + f_2v^2 + f_3v^3 + \mathcal{O}(v^4)], \tag{30a}$$

$$z' = \sqrt{\varepsilon} \left(\frac{\tilde{\omega}_2}{2} g_{11}v + \tilde{w} + \mathcal{O}(\sqrt{\varepsilon}v, \sqrt{\varepsilon}z, \sqrt{\varepsilon}\tilde{w}, v^2) \right), \tag{30b}$$

$$\begin{aligned} \tilde{w}' &= \varepsilon^{3/2} \{ \sqrt{\varepsilon} \nu(\tilde{\mu}, \sqrt{\varepsilon}) - [2\omega_1 + \mathcal{O}(\sqrt{\varepsilon})] \tilde{\mu} \tilde{w} \\ &\quad + \sqrt{\varepsilon} [\omega_1 \tilde{\omega}_2 + \mathcal{O}(\sqrt{\varepsilon})] \tilde{\mu}^2 z \}, \end{aligned} \tag{30c}$$

where

$$\nu(\tilde{\mu}, \sqrt{\varepsilon}) = \omega_1 \tilde{\omega}_2 \tilde{\mu} [\tilde{\gamma} - f(v^-) \tilde{\mu}] + \mathcal{O}(\sqrt{\varepsilon}). \tag{31}$$

Note that Eqs. (30a)–(30c) are a fast-slow system with three distinct time scales, and that the structure of the equations is similar to that of Eqs. (5a)–(5c); the major difference lies in the powers of ε that occur, and in their respective ratios. Nevertheless, as we will show below, the approach developed in Ref. 7 can again be applied in the analysis of Eqs. (30a)–(30c). In particular, the two-dimensional (v, z) subsystem in Eqs. (30a)–(30c), which is to leading order given by

$$v' = a(E_2 - v^- - v)(-z + f_2 v^2 + f_3 v^3), \tag{32}$$

$$z' = \sqrt{\varepsilon} \left(\frac{\tilde{\omega}_2}{2} g_{11} v + \tilde{w} \right),$$

with \tilde{w} treated as a parameter, is a system that undergoes a classical canard explosion at $\tilde{w}=0$.²²

Remark 4. The introduction of \tilde{w} makes the connection between Eqs. (30a)–(30c) and (5a)–(5c) immediate; more precisely, Eq. (30b) shows that \tilde{w} , and not w , is the slowly varying “canard parameter;” see Ref. 7 for details.

B. Dynamics of Eqs. (30a)–(30c) close to ℓ^-

To analyze Eqs. (30a)–(30c) in a neighborhood of the fold line ℓ^- , we need to rescale the equations once again; this is due to the fact that the scale separation in Eqs. (30a)–(30c) breaks down near ℓ^- , which implies a loss of normal hyperbolicity.¹⁴ The required rescaling is analogous to that in Ref. 7, Eq. (2.2), except for the fact that the corresponding powers of ε must be adjusted to the context of Eqs. (30a)–(30c),

$$v = \varepsilon^{1/4} \bar{v}, \quad z = \sqrt{\varepsilon} \bar{z}, \quad \tilde{w} = \varepsilon^{1/4} \bar{w}. \tag{33}$$

[Note that Eq. (33) is one specific realization of the more general technique of geometric desingularization, or blow-up, that has been applied successfully in numerous situations where hyperbolicity is lost; see, e.g., Refs. 16 and 22 for details.]

We now carry out Eq. (33) and subsequently cancel a factor of $\varepsilon^{1/4}$ from the right-hand sides of the resulting equations, which corresponds to a rescaling of time, to obtain the following system:

$$\begin{aligned} \bar{v}' &= a(E_2 - v^-) \left[-\bar{z} + f_2 \bar{v}^2 + \varepsilon^{1/4} \left(f_3 - \frac{f_2}{E_2 - v^-} \right) \bar{v}^3 \right. \\ &\quad \left. + \varepsilon^{1/4} \frac{1}{E_2 - v^-} \bar{v} \bar{z} + \mathcal{O}(\varepsilon^{1/2} \bar{v}^4) \right], \end{aligned} \tag{34a}$$

$$\bar{z}' = \frac{\tilde{\omega}_2}{2} g_{11} \bar{v} + \bar{w} + \mathcal{O}(\sqrt{\varepsilon} \bar{v}, \varepsilon^{3/4} \bar{z}, \sqrt{\varepsilon} \bar{w}, \varepsilon^{1/4} \bar{v}^2), \tag{34b}$$

$$\begin{aligned} \bar{w}' &= \varepsilon \{ \sqrt{\varepsilon} \nu(\tilde{\mu}, \sqrt{\varepsilon}) - \varepsilon^{1/4} [2\omega_1 + \mathcal{O}(\sqrt{\varepsilon})] \tilde{\mu} \bar{w} \\ &\quad + \varepsilon [\omega_1 \tilde{\omega}_2 + \mathcal{O}(\sqrt{\varepsilon})] \tilde{\mu}^2 \bar{z} \}. \end{aligned} \tag{34c}$$

As in Ref. 7, the effect of Eq. (33) on Eqs. (30a)–(30c) is to eliminate the scale separation between v and z , and to unlock the near-integrable structure of the dynamics in the fold region. More precisely, for $\varepsilon=0=\bar{w}$, the (\bar{v}, \bar{z}) subsystem

$$\bar{v}' = a(E_2 - v^-)(-\bar{z} + f_2 \bar{v}^2), \tag{35}$$

$$\bar{z}' = \frac{\tilde{\omega}_2}{2} g_{11} \bar{v}$$

of Eqs. (34a)–(34c) is integrable, with a constant of motion H that can be found in analogy to Ref. 7, Eq. (2.5),

$$\begin{aligned} H(\bar{v}, \bar{z}) &= \frac{\tilde{\omega}_2}{4} g_{11} e^{-4[a(E_2 - v^-)/(\tilde{\omega}_2 g_{11})]f_2 \bar{z}} \\ &\quad \times \left(-\bar{v}^2 + \frac{1}{f_2} \bar{z} + \frac{\tilde{\omega}_2 g_{11}}{4a(E_2 - v^-)f_2^2} \right). \end{aligned}$$

Correspondingly, the orbits of Eq. (35) are determined by the level curves of H , i.e., by $H(\bar{v}, \bar{z})=h$ constant.

We will require the following notation; the reader is referred to Ref. 7, Sec. 2.2 for details. For $\varepsilon > 0$ and a given h value, let $\bar{\gamma}_\varepsilon^h(t) = (\bar{v}, \bar{z}, \bar{w})(t)$ denote the corresponding solution to Eqs. (34a)–(34c), and let $\bar{\Delta}_-$ be the section for the flow of Eqs. (34a)–(34c) defined by $\bar{v}=0$ and $\bar{z}<0$. [Here and in the following, barred quantities denote objects after the rescaling in Eq. (33), i.e., in the new $(\bar{v}, \bar{z}, \bar{w})$ coordinates.] Note that for $h \in (-h_0, h_0)$, with $h_0 > 0$ sufficiently small, $\bar{\gamma}_\varepsilon^h$ can be parametrized by h , in the sense that to any such h there corresponds precisely one value of \bar{z} in $\bar{\Delta}_-$.

For $\varepsilon=0=\bar{w}$ and h fixed, denote by $\bar{\gamma}_0^h(t)$ the solution of the singular equations in Eq. (35) with $H(\bar{v}, \bar{z})=h$, and note that the corresponding orbit will be a closed level curve of H for $h > 0$, respectively, an open one for $h < 0$; typical such curves are illustrated in Fig. 5(a). Now, given $h > 0$, let the time parametrization of $\bar{\gamma}_0^h$ be chosen such that $\bar{\gamma}_0^h(-T^h) = \bar{\gamma}_0^h(T^h)$ lies in $\bar{\Delta}_-$ for some $T^h > 0$, and note that one can show

$$T^h = \frac{2}{\sqrt{a(E_2 - v^-) \tilde{\omega}_2 g_{11}}} \sqrt{-\ln h} + \mathcal{O}(1), \tag{36}$$

in analogy to Ref. 7, Appendix A. The associated (closed) orbits of Eq. (35) are singular templates for the small-amplitude component of the mixed-mode patterns observed in Eqs. (30a)–(30c); cf. again Fig. 5(a). For $\varepsilon > 0$, these orbits will “break up” and perturb as indicated in Fig. 5(b).

Finally, the parabolic orbit of $\bar{\gamma}_0^0(t) = (\bar{v}_0^0, \bar{z}_0^0)(t)$, which is the solution to Eq. (35) obtained for $h=0$, corresponds precisely to the so-called *strong canard* in the limit as $\varepsilon \rightarrow 0$. This strong canard, which will be denoted by Γ_ε^0 , is a trajectory that lies in the transverse intersection of the continuation of $\mathcal{S}_\varepsilon^{a-}$ and $\mathcal{S}_\varepsilon^r$ into the fold region under the flow of Eqs. (30a)–(30c), thereby connecting these two sheets of the slow manifold \mathcal{S}_ε . [As shown in Ref. 7, Γ_ε^0 is well defined in the context of Eqs. (30a)–(30c) once \mathcal{S}_ε is chosen, uniquely up to

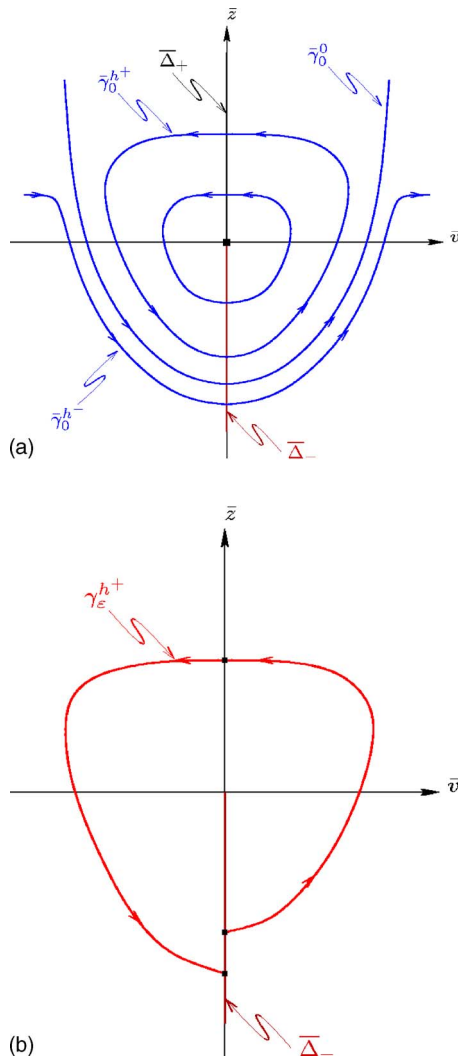


FIG. 5. (Color online) Dynamics of the rescaled system (34a)–(34c): (a) $\epsilon = 0$; (b) $\epsilon > 0$.

exponentially small terms in ϵ .] The strong canard is important insofar as it separates the small-amplitude regime in Eqs. (30a)–(30c) from the relaxation regime; in other words, it “organizes”⁷ the mixed-mode dynamics of Eqs. (30a)–(30c).

C. Global return mechanism

We now discuss the global return mechanism for Eqs. (28a)–(28c), which describes the dynamics away from the fold lines ℓ^\pm , without making specific assumptions about the intrinsic frequencies ω_1 and ω_2 . We will only assume that $\omega_2 > \omega_1$ for the moment; the assumption that $\omega_1 \ll \omega_2$, which has been used extensively in our analysis so far, is not required for the following argumentation.

First, we claim that the transition from steady-state to oscillatory behavior occurs for $\mu = \gamma/f(v^-)$ in Eqs. (28a)–(28c). To that end, we note that Eq. (28c) has an equilibrium that is stable, as well as that the corresponding equilibrium of the full system (28a)–(28c) loses stability through a Hopf bifurcation as $\gamma - \mu f(v^-)$ passes through 0 [or, alternatively, as τ passes through τ_{sn} , cf. Eq. (27)].

Next, we derive an asymptotic formula for the global return and discuss its dependence on $\omega_2 - \omega_1$ as well as the implications for the mixed-mode dynamics of Eqs. (28a)–(28c). Due to the presence of a μ factor, the terms

$$-\frac{\omega_1^2 + \omega_2^2}{\omega_1 + \omega_2} \mu z \quad \text{and} \quad -\frac{\omega_1 - \omega_2}{2} \mu w$$

in Eq. (28b) are small compared to $\bar{\omega}[g_{11}v + \mathcal{O}(v^2)]$ and can hence be neglected. Using a similar argument to that in Ref. 7, Sec. 2.5, we then obtain a first-order equation that describes the global return to leading order,

$$\frac{dw}{dv} = \Psi_0(v)w + \Psi_1(v), \tag{37}$$

with

$$\Psi_0(v) = -\frac{\omega_1 \omega_2}{\bar{\omega}_2} \mu \frac{f'(v^- + v)}{g(v)}$$

and

$$\Psi_1(v) = 2 \frac{\omega_1 \omega_2 f'(v^- + v)}{\bar{\omega}} \frac{1}{g(v)} \left(\frac{-\gamma + f(v^-) \mu}{\omega_1 - \omega_2} - \frac{\omega_1 - \omega_2}{(\omega_1 + \omega_2)^2} \mu [f(v^- + v) - f(v^-)] \right),$$

where g is defined as $g(v) = (E_1 - v)[g_1(v^- + v) - g_1(v^-)]$. The exact solution of Eq. (37), which allows us to express w as a function of v , is given by

$$w(v) = \exp \left[\int_{v^*}^v \Psi_0(\sigma) d\sigma \right] w^* + \int_{v^*}^v \exp \left[- \int_{v^*}^{\sigma} \Psi_0(\sigma') d\sigma' \right] \Psi_1(\sigma) d\sigma, \tag{38}$$

where $w^* = w(v^*)$. For the sake of simplicity, we only consider the leading-order approximation in μ of Eq. (38). Since we want to assume that we have passed the onset of oscillation, i.e., that $\gamma - \mu f(v^-) > 0$, it follows that $\gamma = \mathcal{O}(\mu)$ and hence, that $\Psi_1(v) = \mathcal{O}(\mu)$. We expand the exponentials in Eq. (38) in μ , retaining only the first-order terms, and set

$$G_1(v^*, v) = \int_{v^*}^v \frac{f'(v^- + v)}{g(v)} dv,$$

$$G_2(v^*, v) = \int_{v^*}^v \frac{f'(v^- + v)}{g(v)} [f(v^- + v) - f(v^-)] dv.$$

Moreover, we neglect the contribution coming from the fast dynamics of Eqs. (28a)–(28c) and approximate Eq. (38) by the corresponding integrals over the two sheets \mathcal{S}_0^{\pm} of the critical manifold \mathcal{S}_0 . The relevant v values are given by v_0 and v_{\max} and by v_{\max}^* and 0, respectively, as specified in Fig. 6; see Ref. 7 for details.

Hence, for given w , we find that the leading-order approximation to the corresponding value \hat{w} obtained after one relaxation cycle is given by

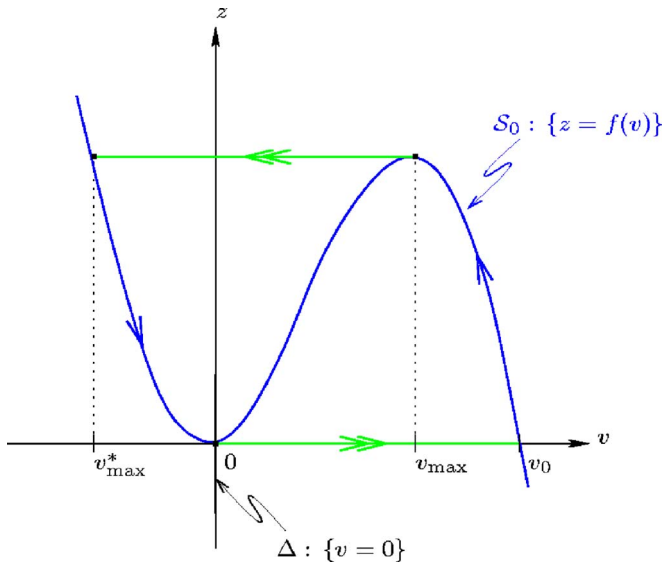


FIG. 6. (Color online) The geometry of the global return.

$$w \mapsto \hat{w} = \left(1 - \frac{\omega_1 \omega_2}{\bar{\omega}_2} \mu [G_1(v_0, v_{\max}) + G_1(v_{\max}^*, 0)] \right) w + 2 \frac{\omega_1 \omega_2}{\bar{\omega}} \left(\frac{-\gamma + f(v^-) \mu}{\omega_1 - \omega_2} [G_1(v_0, v_{\max}) + G_1(v_{\max}^*, 0)] - \mu \frac{\omega_1 - \omega_2}{(\omega_1 + \omega_2)^2} [G_2(v_0, v_{\max}) + G_2(v_{\max}^*, 0)] \right). \quad (39)$$

The asymptotic formula in Eq. (39) describes the global (relaxation) dynamics away from ℓ^\pm that naturally corresponds to the large-amplitude component (“spiking”) of the mixed-mode patterns found in Eqs. (28a)–(28c).

Next, we recall that these patterns arise via slow passage through a canard explosion at $w=0$ in Eqs. (28a)–(28c), with the strong canard Γ_ε^0 acting as the separatrix between nontrivial mixed-mode behavior (where $w < 0$) and the pure relaxation regime, with $w > 0$. Hence, for mixed-mode dynamics to be possible, the global return mechanism must generate $\hat{w} < 0$ from $w > 0$, i.e., the w independent term in Eq. (39) must be negative. More precisely, the critical μ value μ^c , which marks the onset of pure relaxation in Eqs. (28a)–(28c) (or, alternatively, the point where nontrivial mixed-mode patterns cease to exist), is defined by the condition

$$\begin{aligned} & \frac{-\gamma + f(v^-) \mu}{\omega_1 - \omega_2} [G_1(v_0, v_{\max}) + G_1(v_{\max}^*, 0)] \\ & = \mu \frac{\omega_1 - \omega_2}{(\omega_1 + \omega_2)^2} [G_2(v_0, v_{\max}) + G_2(v_{\max}^*, 0)] \end{aligned} \quad (40)$$

to leading order. An approximation for μ^c can be obtained by solving Eq. (40) for μ . For the parameter values specified in the Appendix, we find $\mu^c \approx 0.1181$ (0.1063, 0.0988) for $\omega_2 = 16$ (4, 1.5), which is in good agreement with numerical estimates, recall Figs. 2–4. More importantly, from the form of Eq. (40), we deduce that $\mu^c - \gamma/f(v^-) = \mathcal{O}[(\omega_2 - \omega_1)^2]$, i.e., as $\omega_2 \rightarrow \omega_1$, the size of the μ interval over which MMOs are observed in Eqs. (28a)–(28c) shrinks to 0. This supports the

conjecture of Ref. 3 that the presence of distal compartments with different diameters (and, hence, varying intrinsic frequencies) underlies the irregular firing that is observed in the dopaminergic neuron *in vivo*.

D. Return map II

To derive the lowest-order description of the return map Π induced by the flow of Eqs. (30a)–(30c), we proceed as in Ref. 7, Sec. 2, i.e., we divide the phase space of Eqs. (30a)–(30c) into four distinct regions. We then describe the return map separately in each of these regions, which correspond to

- (i) the dynamics in an $\mathcal{O}(\varepsilon^{1/4})$ neighborhood of the fold ℓ^- (Sec. III B);
- (ii) the entry into this fold region;
- (iii) the exit away from the fold;
- (iv) and the global relaxation mechanism (Sec. III C).

The asymptotic estimates obtained for the return map Π locally in each of the four regions can then be combined into a global, composite formula. The map Π is defined on the (two-dimensional) Poincaré section Δ , which is given by $\{v=0\}$, cf. again Fig. 6, and is most conveniently formulated as a function of (h, \bar{w}) . Since the analysis of Ref. 7 carries over almost verbatim to the context of Eqs. (30a)–(30c), we will only sketch the argument here; the reader is referred to Ref. 7 for details.

The centerpiece of our analysis consists of the asymptotic description of Π close to ℓ^- , see (i); the corresponding local return map will be denoted by $\bar{\Pi}: \bar{\Delta}_- \rightarrow \bar{\Delta}_-$. To that end, we have to consider a suitably truncated approximation for Eqs. (30a)–(30c); we first truncate Eq. (34c) as follows:

$$\bar{w}' = -2\omega_1 \tilde{\mu} \varepsilon^{5/4} \bar{w} + \varepsilon^{3/2} \nu(\tilde{\mu}, 0).$$

Although this approximation is different from the one used in Ref. 7, Sec. 3.3, the following simple observation still enables us to follow closely the development in Ref. 7: A solution $x(t)$ of the linear equation $\dot{x} = ax + b$ with $x(0) = x_0$ is well-approximated by its linearization if $t \in [0, T]$ is such that at is small; namely, $x(t) \approx x_0(1 + at) + bt$. Under the additional (generic) assumption that $h = \mathcal{O}(\varepsilon^M)$ for some $M > 0$, it can be shown that $t \in [0, \mathcal{O}(-\ln \varepsilon)]$ here, see Ref. 7 as well as Eq. (36); hence, the requirement of at small is equivalent to requiring that $\varepsilon^{5/4} \ln \varepsilon$ be small, which is certainly the case. Consequently, again in close analogy to Ref. 7, Sec. 3.3, one can show that the following truncation of Eqs. (34a)–(34c):

$$\begin{aligned} \bar{v}' &= a(E_2 - v^-) \left[-\bar{z} + f_2 \bar{v}^2 + \varepsilon^{1/4} \left(f_3 - \frac{f_2}{E_2 - v^-} \right) \bar{v}^3 \right], \\ \bar{z}' &= \frac{\bar{\omega}_2}{2} g_{11} \bar{v} + \bar{w}(t), \end{aligned} \quad (41)$$

$$\bar{w}(t) = \bar{w} - 2\omega_1 \tilde{\mu} \varepsilon^{5/4} \bar{w} t + \varepsilon^{3/2} \nu(\tilde{\mu}, 0) t,$$

is sufficiently accurate for deriving the lowest-order approximation to $\bar{\Pi}$; a complete justification is beyond the scope of

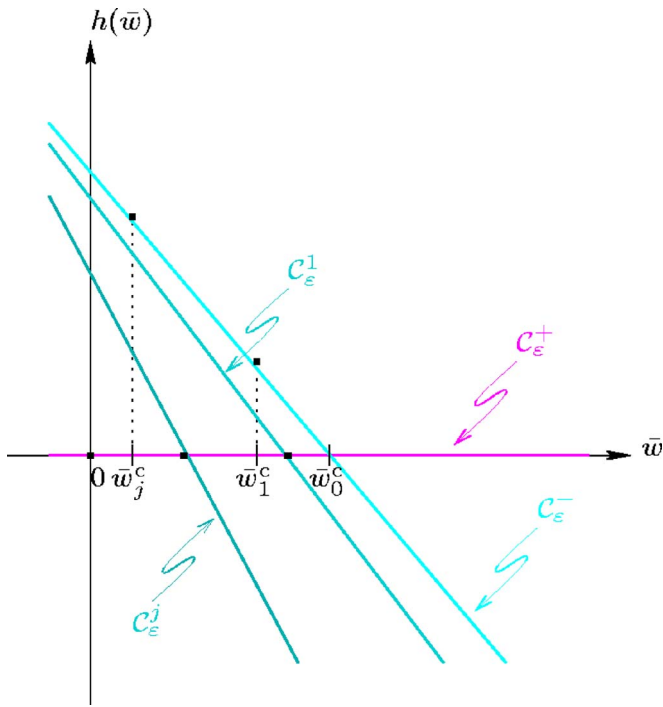


FIG. 7. (Color online) The curves C_ϵ^j for $j \geq 0$ ($C_\epsilon^- \equiv C_\epsilon^0$).

this article. [Here, we have written $\bar{w}(0) = \bar{w}$.]

Furthermore, the curves C_ϵ^- and C_ϵ^+ , respectively, can be defined analogously as in Ref. 7 as the intersection of the continuation of \mathcal{S}_ϵ^- and \mathcal{S}_ϵ^+ , respectively, under the flow of Eqs. (34a)–(34c) with Δ . Similarly, for $j \geq 1$, the curve C_ϵ^j is defined as the image of C_ϵ^- under $\bar{\Pi}^j$, the j th iterate of $\bar{\Pi}$, in $\bar{\Delta}$. As in Ref. 7, one finds that for $j \geq 1$, C_ϵ^j can be written as the graph of a function $h^j(\bar{w})$ for $|\bar{w}|$ sufficiently small. Moreover, h^j is approximately linear in \bar{w} ; see Fig. 7.

The global return mechanism in (iv), on the other hand, can be described to leading order by a formula that is obtained from Eq. (39) via the rescalings introduced in Sec. III B: Given Eq. (29) and, in particular, the assumption that $\omega_1 \ll \omega_2$, Eq. (39) reduces to the following expression for the global return, which we denote by Π^{ret} :

$$\begin{aligned} \bar{w} \mapsto \hat{w} = & \left\{ 1 - 4 \frac{\omega_1}{\omega_2} \tilde{\mu} \epsilon [1 + \mathcal{O}(\sqrt{\epsilon})] [G_1(v_0, v_{\max}) \right. \\ & \left. + G_1(v_{\max}^*, 0)] \right\} \bar{w} + 2\omega_1 \tilde{\mu} \epsilon^{3/2} \{ [\tilde{\gamma} - f(v^-) \tilde{\mu}] \\ & \times [1 + \mathcal{O}(\sqrt{\epsilon})] [G_1(v_0, v_{\max}) + G_1(v_{\max}^*, 0)] \\ & \left. + \tilde{\mu} [1 + \mathcal{O}(\sqrt{\epsilon})] [G_2(v_0, v_{\max}) + G_2(v_{\max}^*, 0)] \right\}; \end{aligned} \quad (42)$$

see also Ref. 7, Eq. (2.53). Here, the integrals in G_i are again defined as in Sec. III C. Recall that Eq. (42) describes the dependence of the return point on $\tilde{\mu}$ after one relaxation cycle, and that the pure relaxation regime has been reached if $\hat{w} = \bar{w}$, i.e., if \bar{w} is mapped onto itself by the global return so that the small-oscillation regime is bypassed. The associated critical $\tilde{\mu}$ value $\tilde{\mu}^c$ can be estimated by solving

$$\begin{aligned} & [\tilde{\gamma} - f(v^-) \tilde{\mu}] [G_1(v_0, v_{\max}) + G_1(v_{\max}^*, 0)] \\ & + \tilde{\mu} [G_2(v_0, v_{\max}) + G_2(v_{\max}^*, 0)] = 0 \end{aligned}$$

for $\tilde{\mu}$, cf. Eq. (40).

Finally, the analysis in the entry and exit regions in (ii) and (iii) can be performed in complete analogy to Ref. 7, Secs. 2.3 and 2.4; the corresponding local maps will be denoted by Π^{in} and Π^{out} , respectively. In sum, the restriction of $\Pi: \Delta \rightarrow \Delta$ to the union of the curves C_ϵ^j ($j \geq 1$) can then be given as follows:

$$\begin{aligned} \Pi(h^j(\bar{w}), \bar{w}) = & \bar{w} + 2[\epsilon^{3/2} \nu(\tilde{\mu}, 0) - 2\omega_1 \tilde{\mu} \epsilon^{5/4} \bar{w}] T^{h^j(\bar{w})} \\ & + \mathcal{O}(\epsilon^{9/4}) \end{aligned} \quad (43)$$

if $h^j(\bar{w}) > 0$ and

$$\begin{aligned} \Pi(h^j(\bar{w}), \bar{w}) = & \left(1 - 4 \frac{\omega_1}{\omega_2} \tilde{\mu} \epsilon \right) \bar{w} \\ & + 2[\epsilon^{3/2} \nu(\tilde{\mu}, 0) - 2\omega_1 \tilde{\mu} \epsilon^{5/4} \bar{w}] T^{h^j(\bar{w}), \text{out}} \\ & - \bar{w} \frac{f_2}{\tilde{\omega}_2 g_{11}} \nu(\tilde{\mu}, 0) \epsilon^{3/2} \ln \epsilon + \mathcal{O}(\epsilon^{5/4}) \end{aligned} \quad (44)$$

if $h^j(\bar{w}) < 0$. Here, $T^{h^j(\bar{w})}$ is defined as in Eq. (36), with h replaced by $h^j(\bar{w})$, and $T^{h^j(\bar{w}), \text{out}} = T^{-h^j(\bar{w})}$.

Finally, we note that the definition of the return map Π depends on the sign of h^j : If $h^j(\bar{w}) > 0$, the point of intersection of the corresponding trajectory of Eqs. (30a)–(30c) with Δ lies above C_ϵ^+ . Hence, the trajectory must remain in the fold region (the small-oscillation regime), and the return to Δ is described by the local map $\bar{\Pi}$ in that case. If, on the other hand, $h^j(\bar{w}) < 0$, i.e., if the trajectory intersects Δ below C_ϵ^+ , it must exit the fold region and undergo a large-amplitude relaxation excursion under the global return. Since, moreover, h^j itself has to be updated after each iteration of Π ,⁷ its sign can change with time, which allows for a transition from small-amplitude “loops” to large-amplitude excursions in Eqs. (30a)–(30c), or vice versa. Hence, in sum, the sign sequence of h^j is in a one-to-one correspondence to the Farey sequence of any given MMO orbit of Eqs. (30a)–(30c). An exemplary illustration of the above mechanism is given in Fig. 8, which shows how the symbolic segment 1^2 is generated by iterating Π .

E. Secondary canards and sectors of rotation

The so-called j th secondary canard Γ_ϵ^j is defined⁷ as a trajectory that undergoes j small (nonrelaxation) rotations, or “loops,” in the fold region before entering relaxation. Then, the values of \bar{w} in C_ϵ^- that correspond to Γ_ϵ^j are determined by finding the points of intersection of subsequent iterates of C_ϵ^- under $\bar{\Pi}$ with C_ϵ^+ . These \bar{w} values will be denoted by \bar{w}_j^c ($j \geq 0$), i.e., the point of intersection of C_ϵ^j with C_ϵ^+ is precisely the image of \bar{w}_j^c under $\bar{\Pi}^j$; see again Fig. 7. The j th sector of rotation RS^j is then defined as the subinterval $(\bar{w}_j^c, \bar{w}_{j-1}^c) \subset C_\epsilon^-$, cf. Fig. 9; this definition can be extended into a neighborhood of C_ϵ^- by the flow of Eqs. (34a)–(34c).

The strong canard Γ_ϵ^0 , with $j=0$, is obtained in the intersection of C_ϵ^- and C_ϵ^+ , i.e., under the zeroth iterate of $\bar{\Pi}$. It can be shown as in Refs. 7 and 22 that the corresponding \bar{w} value

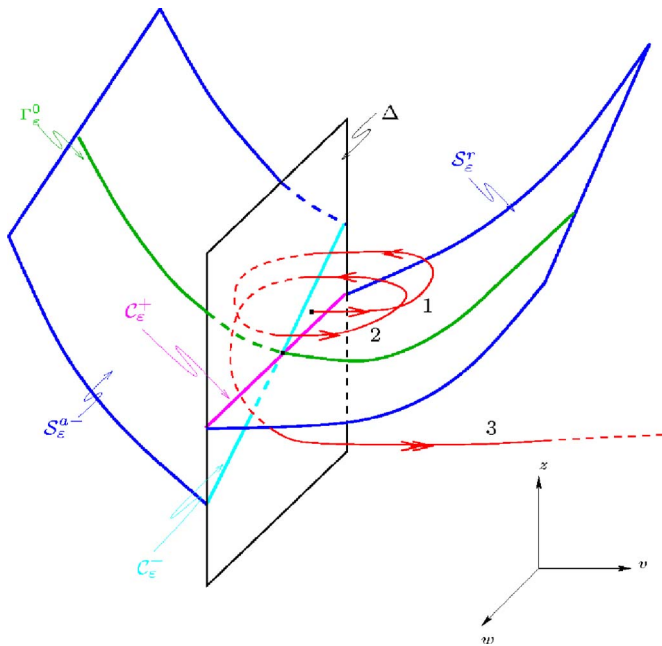


FIG. 8. (Color online) The generation of mixed-mode dynamics by Π .

\bar{w}_0^c is to lowest order determined by solving the condition $d_w^0 \bar{w} + d_\varepsilon^0 \varepsilon^{1/4} = 0$ for \bar{w} . Here, the coefficients d_w^0 and d_ε^0 are given by

$$d_\varepsilon^0 = \int_{-\infty}^{\infty} \nabla H(\bar{\gamma}_0^0(t)) \cdot (a[(E_2 - v^-)f_3 - f_2] \bar{v}_0^0(t)^3 + a \bar{v}_0^0(t) \bar{z}_0^0(t), g_{12} \bar{v}_0^0(t)^2)^T dt, \tag{45a}$$

$$d_w^0 = \int_{-\infty}^{\infty} \nabla H(\bar{\gamma}_0^0(t)) \cdot (0, 1)^T dt, \tag{45b}$$

cf. also Ref. 7, Proposition 2.2, with H and $\bar{\gamma}_0^0$ defined as above and g_{12} the second-order coefficient in the expansion of $g_1(v)(E_1 - v)$ about v^- . The integrals in Eqs. (45a) and (45b) can be evaluated exactly,^{7,22} in particular, it follows that

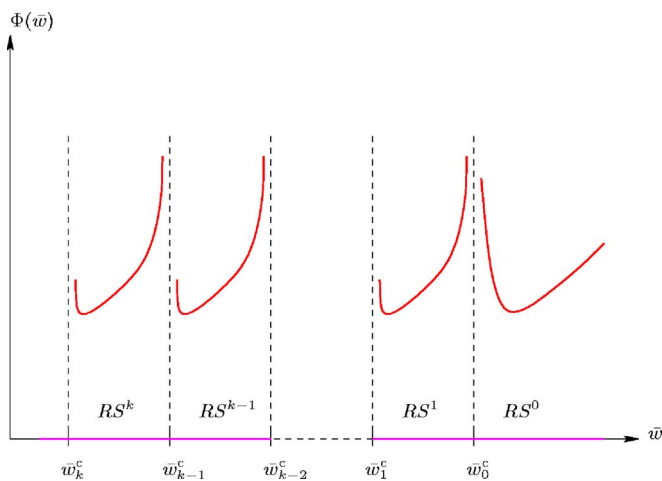


FIG. 9. (Color online) The reduced return map Φ .

$$\bar{w}_0^c = -\frac{d_\varepsilon^0}{d_w^0} \varepsilon^{1/4} + \mathcal{O}(\varepsilon^{1/2}). \tag{46}$$

Similarly, to determine the \bar{w} value \bar{w}_1^c corresponding to the first secondary canard Γ_ε^1 , we have to find the point of intersection of C_ε^1 with C_ε^+ . As it turns out, the corresponding defining condition for \bar{w}_1^c derived in Ref. 7, Eq. (3.21), will now have the form

$$P_h \bar{\Pi}_0(h^0(\bar{w}), \bar{w}) = -[\varepsilon^{3/2} \nu(\bar{\mu}, 0) - 2\omega_1 \bar{\mu} \varepsilon^{5/4} \bar{w}] \mathcal{K}(h^0(\bar{w})) + \mathcal{O}(\varepsilon^{9/4}). \tag{47}$$

Here, h^0 is the value of h corresponding to $\bar{w} \in C_\varepsilon^-$, P_h denotes the projection onto the h coordinate, and $\bar{\Pi}_0$ is the transition map for the simplified truncated system that is obtained for $\bar{w}(t) \equiv \bar{w}$ constant in Eqs. (41). By way of an analogous computation as in Ref. 7, it can be shown that $\mathcal{K}(h) = 2d_w^0 T^h + \mathcal{O}(1)$, where d_w^0 is defined in Eq. (45b).

Then, proceeding as in the proof of Proposition 3.2 in Ref. 7, we find

$$\bar{w}_1^c = \bar{w}_0^c - 2[\varepsilon^{3/2} \nu(\bar{\mu}, 0) - 2\omega_1 \bar{\mu} \varepsilon^{5/4} \bar{w}_0^c] T^{h(\bar{w}_1^c)} + \mathcal{O}(\varepsilon^{9/4}), \tag{48}$$

or, by combining Eqs. (46) and (48),

$$\bar{w}_1^c = \bar{w}_0^c - 2\varepsilon^{3/2} \left(\nu(\bar{\mu}, 0) + 2\omega_1 \bar{\mu} \frac{d_\varepsilon^0}{d_w^0} \right) T^{h(\bar{w}_1^c)} + \mathcal{O}(\varepsilon^{7/4}). \tag{49}$$

Now, from an *a posteriori* argument as in Ref. 7, Sec. 3.3, it follows that $h^j(\bar{w}_1^c) = \mathcal{O}(\varepsilon^{3/2} \sqrt{-\ln \varepsilon})$, which, together with Eq. (36), implies that the lowest-order approximation for the sector width $\Delta \bar{w} := \bar{w}_1^c - \bar{w}_0^c$ is given by

$$\Delta \bar{w} = -\frac{2\sqrt{6} \left[\nu(\bar{\mu}, 0) + 2\omega_1 \bar{\mu} \frac{d_\varepsilon^0}{d_w^0} \right]}{\sqrt{a(E_2 - v^-) \bar{\omega}_2 g_{11}}} \varepsilon^{3/2} \sqrt{-\ln \varepsilon}.$$

Therefore, $\Delta \bar{w} = \mathcal{O}(\varepsilon^{3/2} \sqrt{-\ln \varepsilon})$; moreover, it can be shown as in Ref. 7 that the size of all rotation sectors will be the same to leading order, i.e., that $\bar{w}_j^c - \bar{w}_{j-1}^c = \mathcal{O}(\varepsilon^{3/2} \sqrt{-\ln \varepsilon})$ for any $j \geq 1$. Finally, since $\Delta \bar{w} < 0$, it follows that the smaller j is, the closer the sector RS^j will lie to Γ_ε^0 ; cf. Fig. 9.

F. Reduced return map Φ

The final step in the analysis of the mixed-mode dynamics of Eqs. (30a)–(30c) consists in a reduction of the two-dimensional return map Π , which is *a priori* defined on $\cup C_\varepsilon^j$, to a simplified, one-dimensional map $\Phi: C_\varepsilon^- \rightarrow C_\varepsilon^-$, with

$$\Phi(\bar{w}) = P_{\bar{w}}(\Pi^{\text{in}} \circ \Pi^{\text{ret}} \circ \Pi^{\text{out}} \circ \bar{\Pi}^k(h^0(\bar{w}), \bar{w}))$$

if $(h^0(\bar{w}), \bar{w}) \in RS^k$. (Here, $P_{\bar{w}}$ denotes the projection onto the \bar{w} coordinate.) The main advantage of this reduction lies in the fact that it reduces the description of the flow induced by Eqs. (30a)–(30c) to the analysis of a one-dimensional map that is defined on the single curve C_ε^- . Moreover, Φ is unimodal on each of the sectors of rotation RS^k and can hence be analyzed using standard techniques. Detailed results on

the dynamics of Φ have been derived in Ref. 7, Sec. 3. All these results can be generalized in a straightforward manner, and adapted to the present context; again, the only difference lies in the powers of ε that will occur. In this subsection, we rederive some of the properties of Φ in the framework of Eqs. (30a)–(30c). A qualitative illustration of Φ can be found in Fig. 9.

One important quantity for our analysis is given by the derivative of Φ with respect to \bar{w} on RS^k , since it allows us to estimate the contraction, or expansion, of the dynamics under Φ . As in Ref. 7, Lemma 3.5, it follows with Eq. (31) that

$$\begin{aligned} \Phi'(\bar{w}) &:= \frac{d\Phi(\bar{w})}{d\bar{w}} = 1 + \varepsilon^{3/2} \left(\nu(\bar{\mu}, 0) + 2\omega_1 \bar{\mu} \frac{d_\varepsilon^0}{d\bar{w}} \right) \\ &\times \left(\sum_{j=0}^{k-1} 2 \frac{dT^{h^j(\bar{w})}}{d\bar{w}} + \frac{dT^{h^k(\bar{w}), \text{out}}}{d\bar{w}} \right) \\ &+ \mathcal{O}(\varepsilon^{5/4} \sqrt{-\ln \varepsilon}). \end{aligned}$$

Arguing as in Ref. 7, Sec. 3.5, and taking into account Eq. (36), we find

$$\begin{aligned} \Phi'(\bar{w}) &= 1 - \varepsilon^{3/2} \frac{\nu(\bar{\mu}, 0) d_\varepsilon^0 + 2\omega_1 \bar{\mu} d_\varepsilon^0}{\sqrt{a(E_2 - v^-)} \bar{\omega}_2 g_{11}} \\ &\times \left(\sum_{j=0}^{k-1} 2(j+1) \frac{1}{h^j(\bar{w}^j)} \frac{1}{\sqrt{-\ln h^j(\bar{w}^j)}} \right. \\ &\left. + (k+1) \frac{1}{h^k(\bar{w}^k)} \frac{1}{\sqrt{-\ln h^k(\bar{w}^k)}} \right) + \mathcal{O}(\varepsilon^{5/4} \sqrt{-\ln \varepsilon}). \end{aligned} \tag{50}$$

Then, making use again of $h^j(\bar{w}^j) = \mathcal{O}(\varepsilon^{3/2} \sqrt{-\ln \varepsilon})$, we can write

$$\frac{1}{\sqrt{-\ln h^j(\bar{w}^j)}} = \frac{\sqrt{2}}{\sqrt{-3 \ln \varepsilon}} [1 + \mathcal{O}(1)]$$

and, hence,

$$\begin{aligned} \Phi'(\bar{w}) &\sim 1 - \frac{\nu(\bar{\mu}, 0) d_\varepsilon^0 + 2\omega_1 \bar{\mu} d_\varepsilon^0}{\sqrt{a(E_2 - v^-)} \bar{\omega}_2 g_{11}} \frac{\sqrt{2} \varepsilon^{3/2}}{\sqrt{-3 \ln \varepsilon}} \\ &\times \left(\sum_{j=0}^{k-1} \frac{2(j+1)}{h^j(\bar{w}^j)} + \frac{k+1}{h^k(\bar{w}^k)} \right). \end{aligned}$$

Finally, using a combination of Eq. (49) and an argument analogous to the one preceding Ref. 7, Eq. (3.33), we obtain

$$\Phi'(\bar{w}) \sim 1 - \frac{\omega_k(\eta)}{6 \ln \varepsilon}, \tag{51}$$

where the function ω_k is defined via

$$\omega_k(\eta) = \sum_{j=0}^{k-1} \frac{1}{(k-j) - \eta} - \frac{1}{2\eta}.$$

Here, $\eta > 0$ for $k=0$ and $\eta \in [0, 1]$ for $k \geq 1$, respectively.

In the following, we summarize some of the main findings of Ref. 7 in the framework of Eqs. (30a)–(30c). Given

that the qualitative dynamics of Φ is exactly as derived in Ref. 7, Sec. 3.6, the corresponding proofs carry over almost unchanged; hence, we omit them here.

The first important result in Ref. 7 concerns the existence and stability of periodic MMO orbits of the type 1^k , i.e., of orbits undergoing one large (relaxation) excursion followed by k small (nonrelaxation) loops. In analogy to Ref. 7, Theorem 3.7, one can show that these orbits will exist and be stable on a $\bar{\mu}$ interval whose width is given to leading order by

$$\Delta \bar{\mu}^k = \mathcal{O}[\varepsilon^{1/4} (-\ln \varepsilon)^{-1/2}] \tag{52}$$

for ε sufficiently small. The proof of Eq. (52) is based on deriving a sufficient condition for $|\Phi'| < 1$ in dependence on $\bar{\mu}$, taking into account that

$$\frac{d\bar{\mu}}{d\bar{w}} = - \frac{\frac{\partial \Phi}{\partial \bar{w}} - 1}{\frac{\partial \Phi}{\partial \mu}} \sim \frac{\omega_k(\nu)}{6 D_{\bar{\mu}} \varepsilon^{5/4} \ln \varepsilon} \tag{53}$$

by Eqs. (42) and (51); here, $D_{\bar{\mu}}$ denotes the $\bar{\mu}$ derivative of the right-hand side in Eq. (42), cf. Ref. 7, Sec. 2.5. Then, integrating Eq. (53) with respect to η and applying the Fundamental Theorem of Calculus, one obtains Eq. (52). Note that Eq. (52) in particular implies that the corresponding μ interval will be of the order $\mathcal{O}[\varepsilon^{3/4} (-\ln \varepsilon)^{-1/2}]$; recall $\mu = \sqrt{\varepsilon} \bar{\mu}$.

Given Eq. (52), it can be shown that Theorems 3.9 and 3.10 from Ref. 7 carry over almost verbatim into the context of Eqs. (30a)–(30c). Recall the definition of the Farey sequence $\{L_j^k\}$ that is associated with the MMO orbit in Eqs. (30a)–(30c) consisting of $L_j \geq 1$ relaxation excursions and $k_j \geq 1$ small (nonrelaxation) oscillations. Then, we conclude as in Ref. 7 that, “generically,”

- (1) for $L_j=1$, orbits must consist of segments of the form 1^k (some number of times in succession), 1^{k-1} (some number of times in succession), and 1^{k-2} preceded by 1^k and followed by 1^{k-1} or 1^k ;
- (2) for $L_j=2$, only segments of the type 2^1 or 2^2 will occur;
- (3) for $L_j \geq 3$, only segments of the form L_j^1 will be observed.

These predictions are confirmed by numerical simulations that are presented in Sec. IV below.

IV. DISCUSSION

In this article, we have analyzed a slightly simplified version of the so-called Wilson-Callaway model^{2,4} from a geometric point of view. We have shown how the model equations that were proposed in the two-compartment case in Ref. 3 can be fitted into the framework of Ref. 7. The only real difference between the detailed asymptotics obtained for Eqs. (5a)–(5c) in Ref. 7 and the formulas derived here lies in the fact that the powers of ε that occur, as well as their respective ratios, are slightly different. Yet, the basic features of the two systems—the three time-scale structure and the presence of a folded saddle-node singularity as well as of one

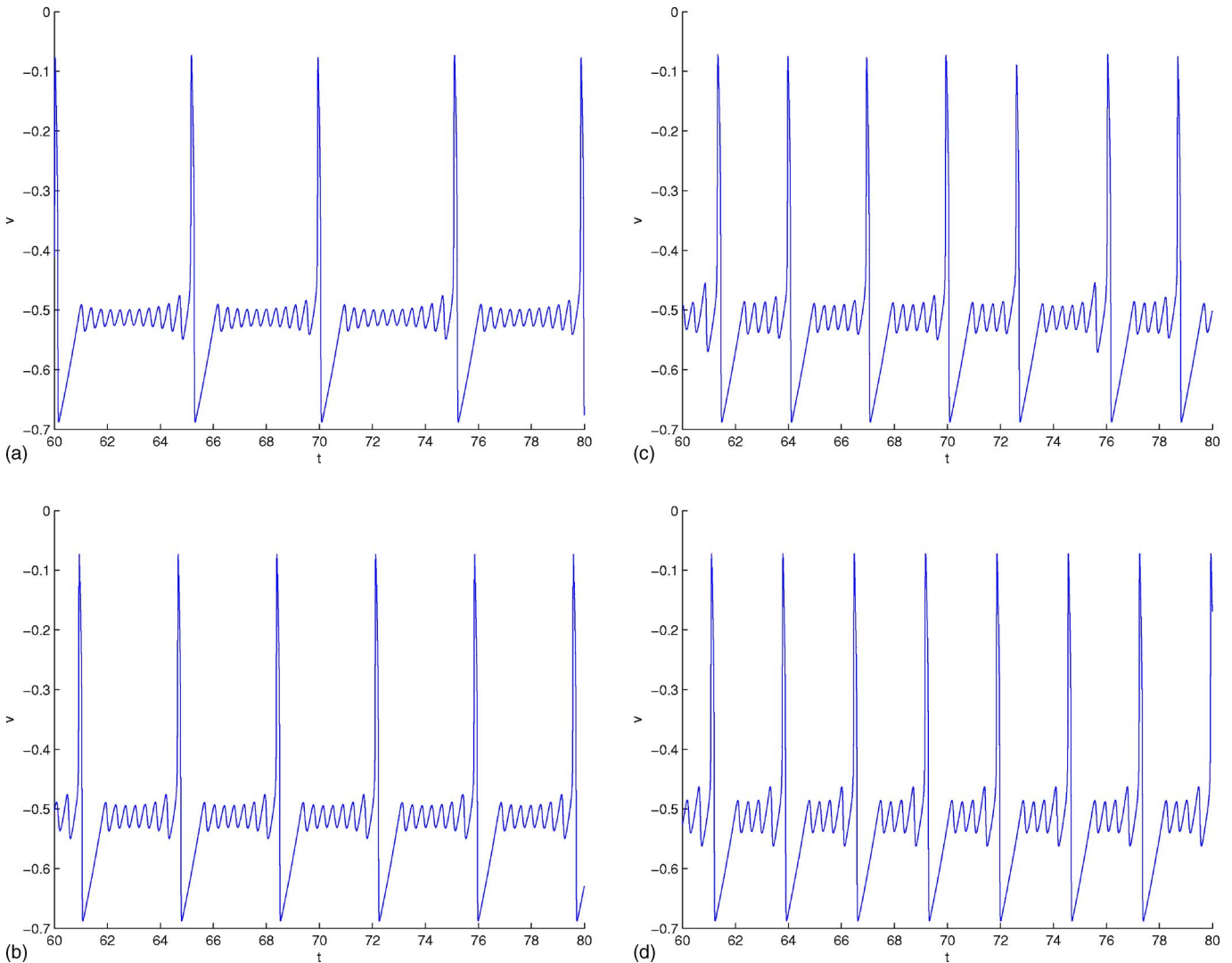


FIG. 10. (Color online) Time series of v in Eqs. (21a)–(21c): (a) $\tau=9.675$; (b) $\tau=9.55$; (c) $\tau=9.425$; (d) $\tau=9.35$. As τ decreases, one observes a transition from (a) $1^{11}1^{10}$ via (b) 1^7 and (c) $1^61^51^4$ to (d) 1^4 in the resulting Farey sequences.

natural bifurcation parameter, say—are the same. Consequently, our results in both cases are qualitatively identical as far as the resulting mixed-mode dynamics is concerned, see Sec. III F. In other words, although the asymptotics obtained here are quantitatively different from those in Ref. 7, the techniques used in the analysis are very similar. There is of course the potential for a more thorough investigation than outlined here; in particular, we emphasize that all the coefficients occurring in our formulas are computable, in the sense that their numerical values are completely determined by the choice of parameters in Eqs. (3a)–(3d), as, e.g., in the Appendix.

Since the present study is largely mathematical, rather than mechanistic, it might be too speculative to try and apply our findings directly to the original, physiological Wilson-Callaway model.² However, two remarks are still in order: First, the bifurcation mechanism, physiologically speaking, is regulated by the rate of calcium efflux from the neuron, which corresponds precisely to the control parameter τ . Upon variation of τ , one can observe varying numbers of subthreshold oscillations. For τ large enough, the oscillatory dynamics breaks down, in agreement with the findings of

Ref. 2, where voltage-gated calcium currents are identified as being essential for sustaining the oscillation.

Second, it is worth pointing out that the results of Sec. III are based on the assumption that the intrinsic frequencies of adjacent neuronal compartments are vastly different, i.e., that $\omega_1 \ll \omega_2$ in our case. If this condition is not satisfied, our analysis of the passage through the fold region is no longer valid. The necessary tools for a more complete analysis are still being developed.⁹ One result we have obtained here is an approximation for the global return mechanism irrespective of the sizes of ω_i , as well as an estimate of the μ interval on which MMOs exist in Eqs. (3a)–(3d); cf. Eq. (40). This estimate leads to the interesting conclusion that the relevant μ range shrinks to zero as $\omega_2 \rightarrow \omega_1$, which can be interpreted physiologically as follows: Studied *in vivo*, the dopaminergic neuron displays three types of oscillatory behavior, regular firing, irregular firing, and bursting.² If MMOs were related to irregular firing sequences, the fact that they vanish for $\omega_2 \rightarrow \omega_1$ would corroborate the conjecture of Ref. 3 that the presence of distal compartments with significantly different natural frequencies is the cause of irregular firing.

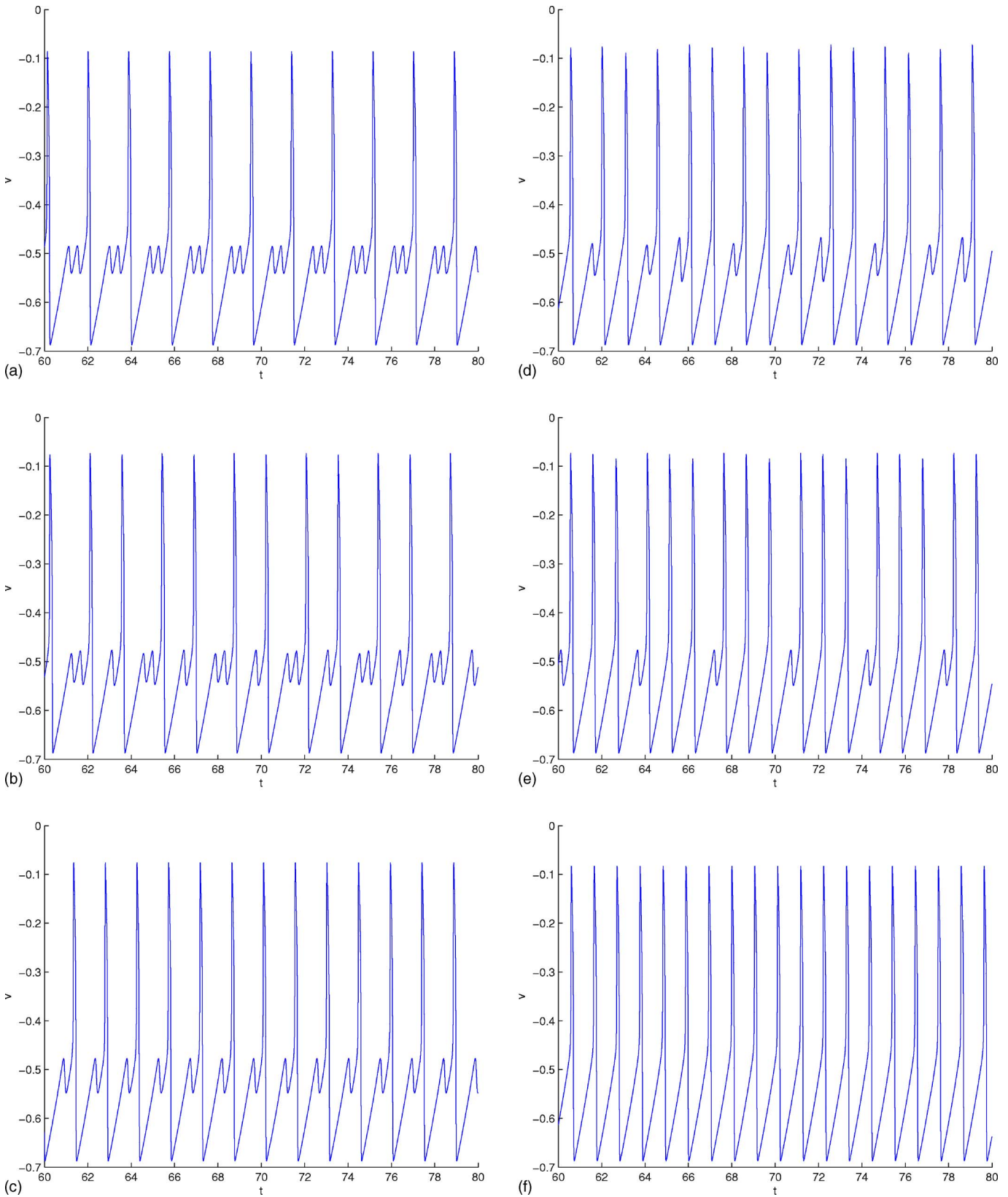


FIG. 11. (Color online) Time series of v in Eqs. (21a)–(21c): (a) $\tau=9.125$; (b) $\tau=9.0$; (c) $\tau=8.875$; (d) $\tau=8.75$; (e) $\tau=8.625$; (f) $\tau=8.5$. As τ decreases, one observes a transition from (a) 1^2 via (b) $1^2 1^1$, (c) 1^1 , (d) $2^1 1^1$, and (e) 3^1 to (f) 1^0 in the resulting Farey sequences.

From a mathematical point of view, one principal result of our analysis is the accurate reduction of the global return map Π , which is defined as a two-dimensional map on the Poincaré section Δ , to a one-dimensional map Φ . The map Φ

is defined on a *set of intervals* (each corresponding to a sector of rotation), approximates Π with an only exponentially small error (in ε), and can be studied using standard techniques.

On the other hand, our analysis also shows that a straightforward reduction of Π to a one-dimensional map defined on a *single* interval is not possible, as postulated by some authors.^{3,5} More precisely, the analysis of Ref. 3 does not resolve the canard structure of system (3a)–(3d) in detail; rather, the Hopf and canard points are “lumped” together into a single point, and this simplification is employed to formulate a piecewise linear return map for Eqs. (3a)–(3d) that is a function of K . Our analysis, on the other hand, resolves the structure between the Hopf point and the canard point in detail. In particular, we show that there exists an entire family of secondary canards in between these points, and that these canards correspond in a unique fashion to the number of small-amplitude “loops” observed in a given MMO trajectory of Eqs. (3a)–(3d), in that they bound the corresponding sectors of rotation. Moreover, the asymptotics of this map Φ can be described in detail to make precise qualitative and quantitative predictions on the admissible Farey sequences, whereas a generic piecewise linear map will allow for a much wider range of possible sequences to occur.

Some of our principal findings from Ref. 7 can be translated into the context of the transformed (v, z, w) system (21a)–(21c) [and, consequently, of the original equations in Eqs. (3a)–(3d)] as follows; details can be found in Ref. 7:

- (i) Sequences of the form $\{1^k\}$ and $\{1^k 1^{k-1}\}$ dominate the stable dynamics; these sequences correspond to MMO trajectories that visit only one and two adjacent sectors, respectively.
- (ii) Segments of the form $L_j^{k_j}$ with $L_j \geq 2$ are not observed when $k_j \geq 2$, except for the segment 2^2 . The segment L_j^1 , however, is admissible for any $L_j \geq 1$.
- (iii) As μ increases, the sequences observed in the transition are roughly of the form $\cdots \rightarrow 1^k \rightarrow 1^k 1^{k-1} \rightarrow 1^{k-1} \rightarrow \cdots$, implying that the dynamics “sweeps through” all sectors of rotation before entering the relaxation regime for $\mu > \mu^c$.
- (iv) The local dynamics depends quite sensitively on the curvature of $f(v)$, i.e., on f_2 , in the sense that 1^k -type orbits become increasingly harder to observe as f_2 increases.
- (v) The number of sectors visited also depends on the strength of the global dynamics, i.e., on how far w is reset after relaxation; by Eq. (42), the corresponding return point will typically be $\mathcal{O}(\varepsilon^{3/2})$ close to the strong canard Γ_ε^0 .
- (vi) The sector width is given by $\Delta \bar{w} = \mathcal{O}(\varepsilon^{3/2} \sqrt{-\ln \varepsilon})$ to leading order, which implies that the global return point will in general lie in one of the lower sectors of rotation, by (v). Hence, one tends to observe a sub-maximum number of small oscillations.
- (vii) The sector size decreases as k increases or, equivalently, as μ decreases; however, we conjecture that the overall dynamics becomes less expanding with higher k , making it less likely for segments of the form $1^k 1^{k-\ell}$, $\ell > 1$, to occur.

With the exception of the conjecture in (vii), these observations are reflected by our numerical findings, cf. Figs. 10 and 11, and are in excellent agreement with the numerical

results obtained in Ref. 3; see, in particular, their Fig. 3. All numerical simulations were performed in MATLAB using the predefined routine ode15s with absolute and relative accuracies 10^{-10} and 10^{-8} , respectively. For clarity, the results are illustrated starting at $t=60$, after initial transients have subsided.

ACKNOWLEDGMENTS

The authors are grateful to Jaime Cisternas, Alexey Kuznetsov, Georgi Medvedev, Björn Sandstede, and Martin Wechselberger for valuable discussions and comments. The research of M.K. was supported in part by National Science Foundation (NSF) Grant No. DMS-0406608. The research of N.P. was supported by NSF Grants Nos. DMS-0109427 (to N.K.), DMS-0211505 (to N.K.), and DMS-0406608 (to M.K.). The research of N.K. was supported in part by NSF Grant No. DMS-0211505.

APPENDIX: PARAMETER VALUES

The parameter values used throughout this article are as follows:

$$E_1 = 1.0, \quad E_2 = -0.9, \quad E_3 = -0.5,$$

$$\bar{g}_1 = 0.8, \quad \bar{g}_2 = 2.0, \quad \bar{g}_3 = 1.0,$$

$$c_1 = -0.35, \quad c_2 = 0.07, \quad c_3 = 1.8,$$

$$\omega_1 = 1.0, \quad \omega_2 = 16.0, \quad \tau = 10.0, \quad d = 4444,$$

$$\varepsilon = 0.013.$$

The linearization of $g_2(u_i)$ about $u_i=2$ is given by $g_2(u_i) \approx -au_i + b$, where the coefficients a and b are fitted to $a = -0.9569$ and $b = -0.7241$, respectively.

Remark 5. Note that the value of c_2 differs from the one cited in Ref. 4, Appendix A; in fact, we did not succeed in obtaining MMOs numerically using the c_2 value from Ref. 3.

¹Y. L. Li, R. Bertram, and J. Rinzel, *Neuroscience* **71**, 397 (1996).

²C. J. Wilson and J. C. Callaway, *J. Neurophysiol.* **83**, 3084 (2000).

³G. S. Medvedev and J. E. Cisternas, *Physica D* **194**, 333 (2004).

⁴G. S. Medvedev, C. J. Wilson, J. C. Callaway, and N. Kopell, *J. Comput. Neurosci.* **15**, 53 (2003).

⁵A. Milik, P. Szmolyan, H. Löffelmann, and E. Gröller, *Int. J. Bifurcation Chaos Appl. Sci. Eng.* **8**, 505 (1998).

⁶M. Brøns, M. Krupa, and M. Wechselberger, *Fields Inst. Commun.* **49**, 39 (2006).

⁷M. Krupa, N. Popović, and N. Kopell (unpublished).

⁸A. Milik and P. Szmolyan, in *Multiple-Time-Scale Dynamical Systems*, edited by C. K. R. T. Jones and A. I. Khibnik, Vol. 122 of IMA Vol. Math. Appl. (Springer-Verlag, New York, 2001), pp. 117–140.

⁹M. Brøns, M. Krupa, and M. Wechselberger (unpublished).

¹⁰M. Wechselberger, *SIAM J. Appl. Dyn. Syst.* **4**, 101 (2005).

¹¹J. Rubin and M. Wechselberger, *Biol. Cybern.* **97**, 5 (2007).

¹²J. Moehlis, *J. Nonlinear Sci.* **12**, 319 (2002).

¹³G. S. Medvedev and N. Kopell, *SIAM J. Appl. Math.* **61**, 1762 (2001).

¹⁴N. Fenichel, *J. Differ. Equations* **31**, 53 (1979).

¹⁵E. Benoit, J.-L. Callot, F. Diener, and M. Diener, *Collect. Math.* **31**, 37 (1981).

¹⁶F. Dumortier, in *Bifurcations and Periodic Orbits of Vector Fields*, edited by D. Schlomiuk, Vol. 408 of NATO ASI Series C: Mathematical and Physical Sciences (Kluwer Academic, Dordrecht, 1993), pp. 19–73.

¹⁷F. Dumortier and R. Roussarie, *Mem. Am. Math. Soc.* **121**, 577 (1996).

¹⁸W. Eckhaus, in *Asymptotic Analysis, II*, edited by F. Verhulst, Vol. 985 of *Lecture Notes in Mathematics* (Springer-Verlag, Berlin, 1983), pp. 449–494.

¹⁹P. Szmolyan and M. Wechselberger, *J. Differ. Equations* **177**, 419 (2001).

²⁰B. Sandstede (private communication).

²¹J. Jalic, M. Krupa, H. G. Rotstein, and N. Kopell (unpublished).

²²M. Krupa and P. Szmolyan, *J. Differ. Equations* **174**, 312 (2001).